ADVANCED ENERGY MATERIALS
www.advenergymat.de

Molecular Understanding of Fullerene – Electron Donor Interactions in Organic Solar Cells

*Sean M. Ryno, Mahesh Kumar Ravva, Xiankai Chen, Haoyuan Li, and Jean-Luc Brédas**

This Review is dedicated to Professor Nazario Martín, an outstanding scientist, wonderful friend, and great fan of Atlético Madrid, at the occasion of his 60th birthday.

Organic solar cells hold promise of providing low-cost, renewable power generation, with current devices providing up to 13% power conversion efficiency. The rational design of more performant systems requires an in-depth understanding of the interactions between the electron donating and electron accepting materials within the active layers of these devices. Here, we explore works that give insight into the intermolecular interactions between electron donors and electron acceptors, and the impact of molecular orientations and environment on these interactions. We highlight, from a theoretical standpoint, the effects of intermolecular interactions on the stability of charge carriers at the donor/acceptor interface and in the bulk and how these interactions influence the nature of the charge transfer states as wells as the charge separation and charge transport processes.

1. Introduction

Organic solar cells (OSC) are promising candidates for low-cost renewable energy production due to their ability to be printed, via high throughput methods, on large-area, flexible substrates. Through years of research involving fullerenes and numerous donor materials as well as engineering of device fabrication techniques, the performance of fullerene-based OSCs have now reached nearly 12% power conversion efficiency (PCE) in single-junction devices,[1] while PCEs of greater than 13% have been reported in proprietary multi-junction devices.[2,3] Despite these efficiencies actually doubling over the past decade, still better performance is necessary for many commercial applications.

Fullerenes, both substituted (e.g., $PC_{61}BM$) and unsubstituted (e.g., C_{60}), are ubiquitous as electron-accepting materials in the active layers of OSCs, with either a small molecule or polymer acting as the electron-donating material. We note, however, that non-fullerene acceptor materials have also recently gained substantial interest; non-fullerene OSCs to date lead to PCEs up to 9.5%,[4] which remains lower that the best fullerene-based devices. The donor materials, both small molecule and polymers, have also seen significant research efforts directed at developing increasingly better performing materials; small-molecule based devices now reach 9.0%[5] while polymer-fullerene devices hold the current record for single-junction devices at 11.7%.[1]

In order to realize increased PCEs, a detailed understanding of the energetic landscape and intermolecular interactions at the interface between the electron donor and the electron acceptor is crucial. Also, the morphology within the active layers, whether in a bilayer structure or a blend (termed a bulk heterojunction (BHJ)), plays a crucial role in the determining the efficiencies of the various electronic and optical processes involved in OSC operation.[6–8] Thus, by better understanding how intermolecular interactions impact these processes and how advantageous characteristics may be obtained by tuning the processing conditions, additional insight can be gained into the rational design of improved organic electronic materials for photovoltaics applications.

In addition, one of the processes central to the operation of OSCs as wells as organic light-emitting diodes and organic thin-film transistors, and often a limiting factor in their performance, is the efficiency with which the active layer can transport generated or injected charges, either holes or electrons. The charge-carrier mobility, the rate at which charges move through a material, is dependent on a number of parameters including the chemical and molecular structure of the material constituents,[9] impurities and defects within the active layer that can act as charge trapping sites that reduce the carrier mobility,[10,11] and the solid-state molecular packing.[12–15]

In this Review, we focus, from a theoretical point of view, on understanding the interactions between fullerene acceptors and small-molecule or polymer donors, how these interactions influence the site energies and charge transfer state energies of the donor and acceptor components at their interfaces in OSCs, what is the effect of delocalization on the site energies and charge transfer states, and, finally, how do these interactions impact the charge separation and charge transport processes. Throughout this Review, we try to highlight how molecular

Dr. S. M. Ryno, Dr. M. K. Ravva, Dr. X.-K. Chen, Dr. H. Y. Li, Prof. J.-L. Brédas
Laboratory for Computational and Theoretical Chemistry of Advanced Materials
KAUST Solar Center
Physical Science and Engineering Division
King Abdullah University of Science and Technology
Thuwal 23599–6900, Kingdom of Saudi Arabia
E-mail: jean-luc.bredas@kaust.edu.sa

DOI: 10.1002/aenm.201601370

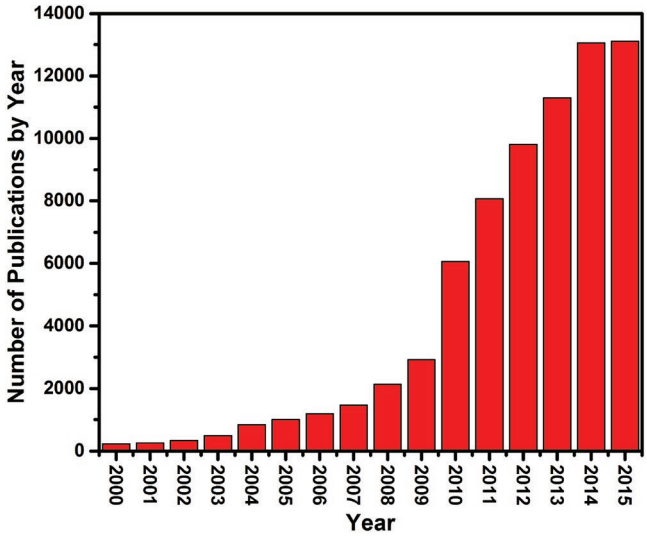

Figure 1. Approximate number of publications relating to organic solar cells and fullerenes. Citation report for "organic solar cells & fullerenes" or "organic photovoltaics & fullerenes" in the publication title or topic. Retrieved from Web of Science on June, 8, 2016.

structure or intermolecular configurations impact the various processes in OSCs to provide some general guidance for materials engineering efforts.

We note that, over the past 15 years, there has been a steady increase in the number of publications discussing OSCs (**Figure 1**), with over 13 000 publications in 2015 alone. As it is thus very challenging to provide a complete overview of the field, we try and select works that specifically relate to an increased understanding of the processes that occur in OSCs as they pertain to intermolecular interactions. In particular, we focus on the factors that impact the site energies at the donor-acceptor interface, on the interactions that dictate the charge transfer state energies and the energetics of charge separation and on charge transport in OSC materials. While our primary focus here is on fullerene systems, it is important to note that these same principles should also apply to non-fullerene moieties. This Review is organized as follows: Section 2 provides a brief reminder of the key processes taking place in OSCs; Section 3 reviews common OSC materials and the interactions within pure donors and acceptors and between donors and acceptors; Section 4 constitutes the primary focus of this Review and discusses the effects of intermolecular interactions and molecular packing on the site energies and charge transfer state energies, the effects of charge carrier delocalization, and how the charge separation and charge transport processes are impacted by molecular interactions; lastly, Section 5 provides outlook and concluding remarks.

2. Brief Reminder of OSC Operation

Over the past couple of decades, there has been continuous work to better understand the processes that occur in OSCs,[7,16–20] which include: optical absorption, exciton formation, exciton migration, exciton dissociation, charge transport, and charge collection. Importantly, charge recombination, which negatively impacts performance through annihilation of

Sean M. Ryno received his Bachelor of Science degree in Chemistry from the University of North Georgia, Dahlonega, Georgia in 2010. He then joined the group of Jean-Luc Brédas at the Georgia Institute of Technology where he received his Ph.D. in Computational Chemistry in 2015. Currently, he is a postdoctoral fellow at King Abdullah University of Science and Technology in the Solar and Photovoltaics Engineering Research Center in the group of Jean-Luc Brédas. His current research interests are focused on understanding the energetics at donor-acceptor interfaces in organic photovoltaics.

Mahesh Kumar Ravva received his Master of Science degree in Chemical Sciences from Pondicherry University, Puducherry, in 2008 and his Ph.D. degree in Chemistry from the University of Madras, Chennai, in 2013 from the group of Venkatesan Subramanian. After a postdoctoral appointment at the Georgia Institute of Technology, he is now working as a postdoctoral fellow at King Abdullah University of Science and Technology in the Solar and Photovoltaics Engineering Research Center in the group of Jean-Luc Brédas. His current research work mainly focuses on understanding the nature of various non-covalent interactions in functional materials using modern computational chemistry methodologies.

Haoyuan Li received a dual BSc degree in chemistry and biotechnology from Jilin University in 2010. He then joined the group of Yong Qiu in the Department of Chemistry at Tsinghua University, where he received his Ph.D. in Chemistry in 2015. He is currently a postdoctoral fellow at King Abdullah University of Science and Technology in the group of Jean-Luc Brédas. His research interests focus on understanding the physics of organic electronics devices.

an electron-hole pair, may also occur after exciton formation or dissociation. To provide a framework for later discussion, and to familiarize readers with terminology, we now briefly describe each of these processes.

The first process to occur in the π-conjugated materials that composes the OSC active layer is the photogeneration of a Coulombically bound electron-hole pair, referred to as an exciton. In order to absorb photons over a significant portion of the solar spectrum, low optical-gap materials have been developed that efficiently absorb photons in the near-IR and often over more than a 1 eV range.[8] Once an electron has been excited, it vibrationally relaxes down to the bottom of the lowest excited-state potential energy surface and an exciton is formed; the energy associated with this excitation (most generally from a singlet electronic ground state, S_0, to the first singlet excited state, S_1) corresponds to the optical gap, E_{opt} (**Figure 2**); due to this vibrational relaxation of the excited electron, excess energy from high-energy incident photons is lost, which acts to reduce the open-circuit voltage, V_{OC}, of OSC devices.[21,22]

In the case of bilayer architectures, the exciton, a neutral species, then randomly diffuses through the active layer, via a series of energy transfer processes, until it reaches the electron donor-electron acceptor interface.[23] During the time of this migration process, excitons may decay back to the ground state before they are able to reach the electron donor-electron acceptor interface where they can dissociate. This is the main reason for the introduction of the BHJ architecture, the excitons being then formed near an interface.[17,24–30] Exciton dissociation leads to the formation of a charge-transfer (CT) state related to an electron transfer from the electron donor component to the electron acceptor component. As will be discussed in Section 4.3, the energy associated with this CT state is intimately dependent on the local molecular configurations (packing) at the donor-acceptor interface. The CT state can then dissociate into a charge separated (CS) state, where the hole and electron move away from one another after having overcome their Coulombic attraction.[31] The charge carriers migrate within the active layer of the devices to their respective electrodes for collection. The rate at which holes and electron migrate through their respective medium is determined by the electronic couplings between relevant molecular orbitals on adjacent molecular sites within the donor and acceptor phases (the highest-occupied molecular orbital (HOMO) for holes and lowest-occupied molecular orbital (LUMO) for electrons).[9] During their migration to the electrodes, a hole and an electron may find one another and reform a CT state at a donor-acceptor interface; from there, they can either again separate into charge carriers or recombine via non-geminate charge recombination.

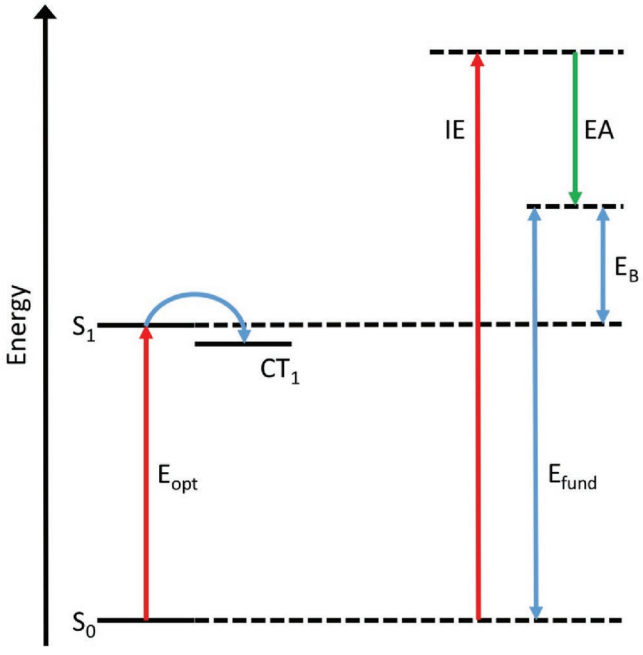

Figure 2. Illustration of the electronic states relevant in the operation of organic solar cells. S_0 is the singlet electronic ground state of the absorbing material (ususally the electron-donor component in the case of fullerene-based OSCs); S_1 is the first singlet excited state of the absorbing material; and CT_1 is the lowest energy charge-transfer state at the donor-acceptor interface. *IE* and *EA* denote the ionization energy and electron affinity, respectively. E_{opt} is the optical gap, considering the S_1-S_0 energy difference; E_{fund} is the fundamental gap, defined as *IE*-*EA*. The exciton binding energy, E_B, is defined as the energy difference between S_1 and E_{fund}.

3. Electron Donor and Electron Acceptor Materials

3.1. Small-Molecule and Polymer Electron Donor Materials

Small molecules, oligomers, and polymers are all used as electron donating materials in OSCs. Although these materials belong to different classes and cover various length scales, the basic electrical and optical properties are similar. An optimal electron donating material should possess strong, broad absorption across the solar spectrum, large hole mobility for efficient and fast charge transport, energy levels that align well and couple strongly with the energy levels of the electron acceptor for efficient charge transfer, and appropriate miscibility with the electron acceptor to form the desired nanoscale morphologies. Various design principles, such as tuning of the energy levels via chemical modification (for instance, via fluorine substitution) and incorporation of alternating electron-rich and electron-poor moieties, have been established to develop new donors with good performance in OSC devices (**Figure 3**).[32–34]

Poly-3-hexylthiophene (P3HT) and other homopolymers have received considerable attention, in particular in the early stages of development. In the case of P3HT, specific synthetic procedures can lead the 3-hexylthiophene monomers to polymerize in a regioregular fashion (only head-to-tail linkages, RR-P3HT) rather than in a regiorandom fashion (head-to-tail, head-to-head, and tail-to-tail linkages, RRa-P3HT).[35,36] The regularity in RR-P3HT acts to reduce the steric interactions among alkyl side-chains and induces better planarity of the backbone and a lower optical gap than in RRa-P3HT.

Incorporating alternating electron-rich ("donor") and electron-poor ("acceptor") moieties is currently one of the prominent strategies to develop low optical-gap polymers and small molecules.[37–40] Using such an approach, a myriad of low optical-gap donor-acceptor co-polymers have been synthesized over the past three decades. Examples of such materials include copolymers based on benzothiadiazole (BT), pyrrolo[3,4-c]pyrrole-1,4-dione

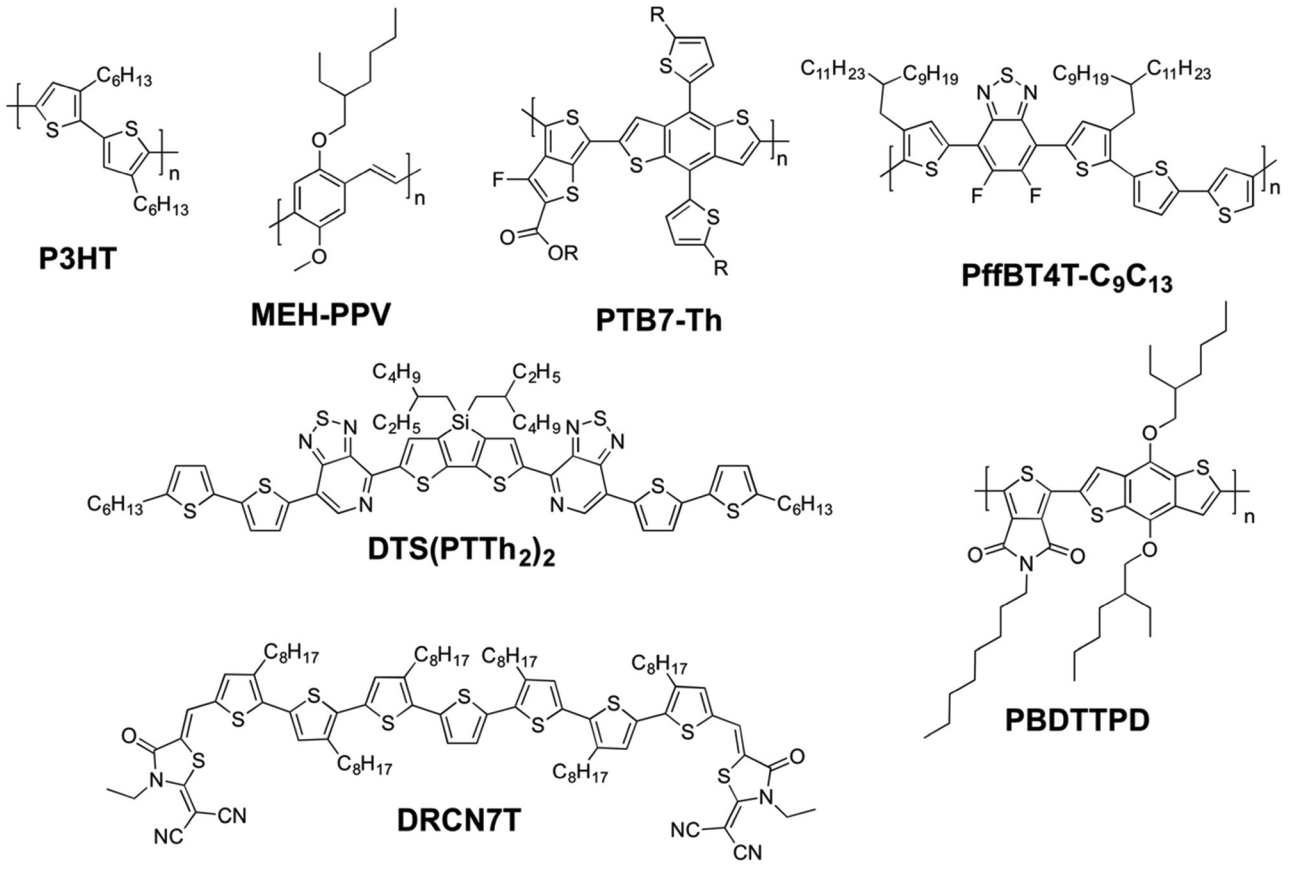

Figure 3. Chemical structures of representative electron donor polymers and small molecules. Structures: poly(3-hexyl-thiophene) (P3HT), Ref. [35]; poly(2-methoxy-5-(2-ethylhexyloxy)-1,4-phenylenevinylene (MEH-PPV), Ref. [252]; poly[[2,6′-4,8-di(5-ethylhexylthienyl)benzo[1,2-*b*;3,3-*b*] dithiophene][3-fluoro-2[(2-ethylhexyl)carbonyl]thieno[3,4-*b*]thiophenediyl]] (PTB7-Th), Ref. [88]; poly[(5,6-difluoro-2,1,3-benzothiadiazol-4,7-diyl)-*alt*-(3,3‴-di(2-nonyltridecyl)-2,2′;5′,2″;5″,2‴-quaterthiophen-5,5‴-diyl)] (PffBT4T-C_9C_{13}), Ref.[1]; 5,5′-*bis*{(4-(7-hexylthiophen-2-yl)thiophen-2-yl)-[1,2,5]thiadiazolo[3,4-c]pyridine}-3,3′-di-2-ethylhexylsilylene-2,2′-bithiophene (DTS($PTTh_2$)$_2$), Ref. [5]; poly(di(2-ethylhexyloxy)benzo[1,2-*b*:4,5-*b*′]dithiophene-*co*-octyltthieno[3,4-*c*]pyrrole-4,6-dione) (PBDTTPD), Ref. [46]; 2,2′-((5Z,5′Z)-5,5′-((3,3‴″,3‴″″,3‴″″″,4′,4″-hexa-octyl-[2,2′:5′,2″:5″,2‴:5‴,2″″:5″″,2‴″″:5‴″″,2‴″″″-sepithiophene]-5,5‴″″″-diyl)bis(methanylylidene))bis(3-ethyl-4-oxothiazolidine-5,2-diylidene))dimalononitrile (DRCN7T), Ref. [253].

(DPP), or benzo[1,2-b;4,5-b′]dithiophene (BDT), to name just a few. The backbone along the copolymer chains is often twisted to various extents due to steric interactions between adjacent rings or side-chains. Since such twists can limit electronic delocalization and widen the optical gap, strategies have also been developed to planarize the backbone, which include: (i) introducing aromatic or vinylene spacers between the donor and acceptor subunits;[41–43] (ii) choosing donor and acceptor units without *ortho*-hydrogen atoms to prevent C-H···H-C steric interactions; (iii) fusing donor and acceptor units to increase the rigidity of the backbone (e.g., ladder polymers);[44] or (iv) fluorination of the polymer backbone. Each of these strategies allows control of some of the (intermolecular) interactions along the polymer chains.

To improve solubility, the π-conjugated polymer chains are often functionalized with alkyl (or alkoxy) side-chains, either linear or branched.[45] Such functionalization strongly impacts the manner in which the polymer chains pack, often limiting their crystallinity. For instance, in the case of PBDTTPD, composed of alternating thieno[3,4-b]thiophene-pyrrole-4,6-dione and benzodithiophene units, crystallite formation and relative backbone orientations very much depend on the pattern of the alkyl side-chains along the backbone.[46] Thus, choosing alkyl side-chains of appropriate nature and length (side-chain engineering) is crucial to the design of efficient electron donor materials. The current champion polymer donor material, poly[(5,6-difluoro-2,1,3-benzothiadiazol-4,7-diyl)] (PffBT4T), leads to devices with nearly 12% efficiency when functionalized with suitable side-chains.[1,47]

While our discussion has focused so far on polymer donor materials used in solution-processable polymer:fullerene BHJ solar cells, small-molecule systems are emerging as a competitive alternative to their polymer counterparts, as highlighted in the Introduction. Compared to polymers, small molecules have several potential advantages that make them attractive materials, such as more versatile molecular structure, simpler strategies for controlling energy levels, and more reproducible synthetic procedures leading to materials of higher purity.

3.2. Electron Acceptor Materials

3.2.1. Fullerenes

The discovery and characterization of fullerene-C_{60} by Kroto et al. has had a major impact on the chemistry and physics

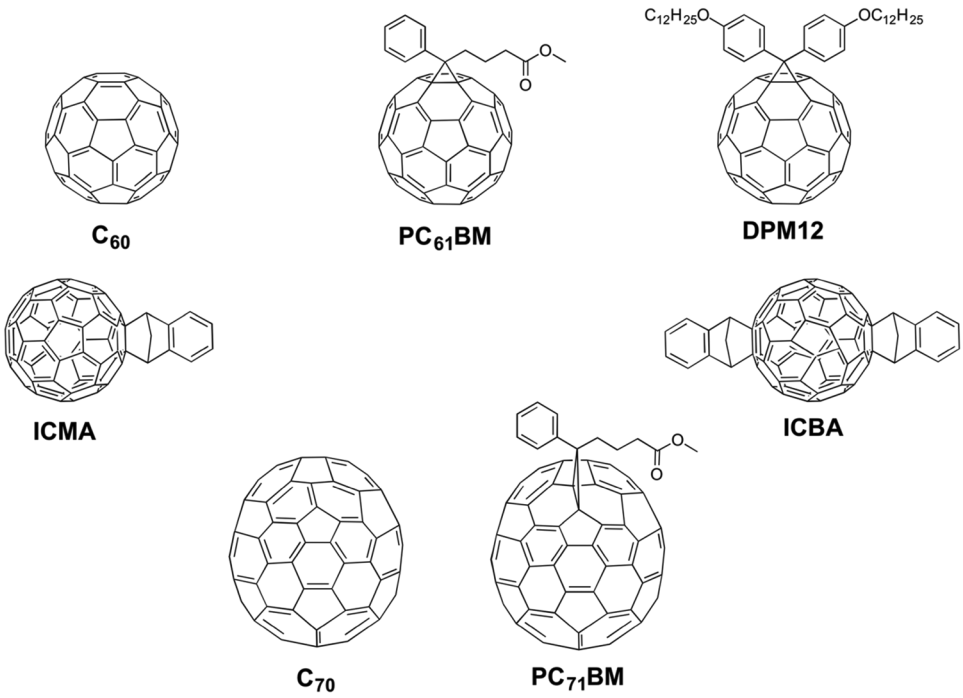

Figure 4. Chemical structures of C_{60}, C_{70}, and representative derivatives. Structures: C_{60}, C_{70}, Ref. [49]; phenyl-C_{61}-butyric acid methyl ester ($PC_{61}BM$), Ref. [254]; diphenylmethanofullerene (DPM12), Ref. [77]; indene-C_{60} monoadduct (ICMA), indene-C_{60} bisadduct (ICBA), Ref. [68]; phenyl-C_{71}-butyric acid methyl ester ($PC_{71}BM$), Ref. [65].

of electron transport materials.[48,49] Following this discovery, Heeger and co-workers demonstrated photo-induced electron transfer from the excited state of poly-paraphenylene vinylene to fullerene,[16] highlighting the electron accepting capabilities of fullerene and their potential for exploitation in organic photovoltaics devices. Among the fullerene family, C_{60} and C_{70} and their derivatives have been extensively studied and widely used as electron accepting materials in OSCs (**Figure 4**). By blending C_{60} or the phenyl-C_{61}-butyric acid methyl ester ($PC_{61}BM$) derivative with a conjugated polymer, Heeger and co-workers and Friend and co-workers showed that efficient power conversion and charge collection were possible in OSCs.[28,29] The high electron affinity of fullerenes, which assists in efficient photo-generation, and their three-dimensional structure, which ensures packing[50–52] that allows for multiple pathways and entropic gain for exciton dissociation[19,53,54] and charge transport,[55] are among their attractive properties for OSCs. The best performing devices currently incorporate a fullerene as the electron acceptor.[1]

The low solubility of C_{60} has limited its application in BHJ solar cells. The chemical functionalization of the fullerene cage has been extensively used to improve solubility in many organic solvents.[56] Since the functionalization destabilizes the LUMO levels (due to partial loss of conjugation), higher open-circuit voltages can be achieved than with bare C_{60}; also, functionalization alters the electron density in the fullerene cage and lowers the molecular symmetry, which induces a dipole moment in the molecule and enhances optical absorption.[57,58] Understanding the impact functionalization has on the interactions among fullerenes and with other molecules, their solubility, and their aggregation properties, is key to determining the factors that influence packing and morphology and to achieving higher power conversion efficiencies.[59]

Of the several fullerene derivatives that have been synthesized and evaluated,[48,56,60–67] $PC_{61}BM$ has been the most widely exploited as an electron accepting material in OSCs.[56,60] C_{70} and its derivatives such as $PC_{71}BM$, in spite of their high cost, have also been used in order to benefit from their higher optical absorption characteristics.[65] However, the elliptical structure of the C_{70} cage leads to the formation of several regioisomers in $PC_{71}BM$, which increases disorder. A series of fullerene mono- and multi-adducts have also been synthesized with the goal of decreasing the electron affinity (and improving V_{OC}).[68–70] Among these, the indene-C_{60} monoadduct (ICMA) and indene-C_{60} bisadduct (ICBA) have received considerable attention, with the electron affinity evolving from 3.91 eV in $PC_{61}BM$ to 3.86 eV and 3.74 eV in ICMA and ICBA, respectively.[68] As with C_{70}, C_{60} bisadduct synthesis often results in several regioisomers whose electronic properties can vary strongly from one isomer to the next. For example, Zhang et al.[71] have shown that the electron affinities estimated via cyclic voltammetry for different regioisomers of *N*-methyl-phenyl-C_{61}-propyl-2-fullero-pyrrolidine, can differ by over 0.1 eV. Xiao et al.[72] have also shown that OSC performance can improve by more than one percentage point by use of select regioisomers. As such, efforts are underway to devise regioselective synthetic pathways.[71–76] Martín and co-workers have developed a number of fullerene-functionalized polymers and small molecules that have resulted in V_{OC} greater than 0.6 V when blended with P3HT, which is larger than the 0.5 V in $PC_{61}BM$ systems with the same donor.[77] Increasing the level of functionalization causes additional reductions in electron affinity, but also disruption of electron delocalization

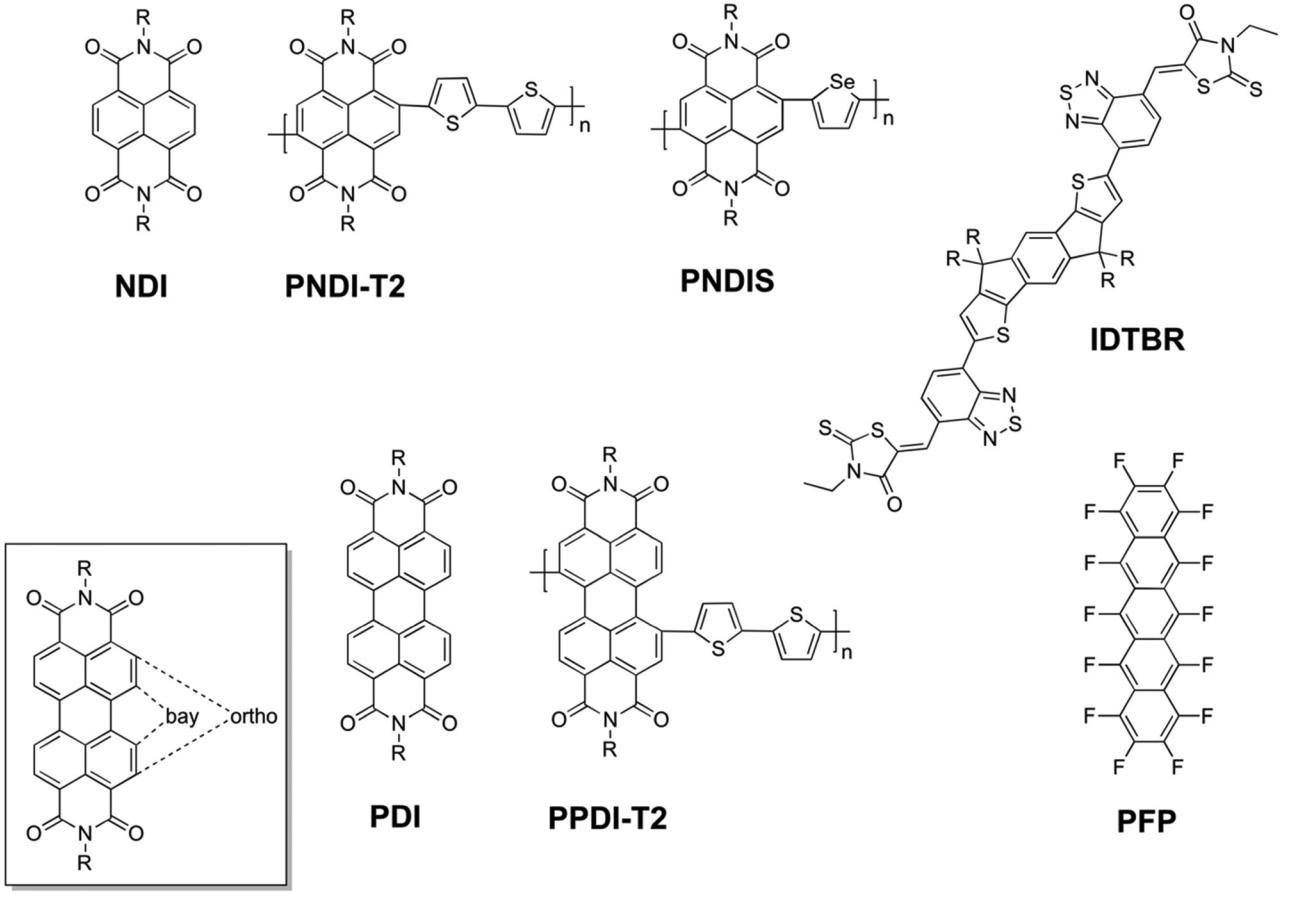

Figure 5. Chemical structures of NDI and PDI small molecules and polymers and representative small-molecule non-fullerene acceptors. (Inset) Substitution positions on PDI. Structures: naphthalene diimide (NDI), perylene diimide (PDI), Ref. [96]; poly([naphthalene-1,4,5,8-bis(dicarboximide)-2,6-diyl]-*alt*-5,5′-(2,2′-bithiophene)) (PNDI-T2), poly([3,4,9,10-perylenedicarboximide-(1,7&1,6)-diyl]-*alt*-5,5′-(2,2′-bithiophene)) (PPDI-T2), Ref. [87]; poly([naphthalene-1,4,5,8-bis(dicarboximide)-2,6-diyl]-*alt*-5,5′-(2-selenophene)) (PNDIS), Ref. [255]; indacenodithiophene-benzothiadiazole-3-ethylrhodanine (IDTBR), Ref. [108]; perfluoropentacene (PFP), Ref. [94].

and packing in the solid state, which can result in poor electron transport.[78–80] Recently, the static disorder (time-independent variations in molecular positions) and dynamic disorder (time-dependent variations due to electron-vibration coupling) were investigated in C_{60}, C_{70}, $PC_{61}BM$, and $PC_{71}BM$, using a combined quantum mechanics and molecular dynamics approach.[81] Tummala et al. found that, in the amorphous phase, the static disorder increases by some 40% in going from C_{60} to C_{70} or $PC_{61}BM$ to $PC_{71}BM$ and is more than doubled for the PCBM derivatives vs the unsubstituted structures; the dynamic disorder also adds a significant contribution in all instances. The resulting distribution in electron affinities has negative impact as it leads to charge carrier relaxation, energy loss, and reduced V_{OC}.

3.2.2. Non-Fullerene Acceptors

Since fullerene acceptors generally suffer from weak absorption in the visible, limited opportunity of optical gap tuning, aggregation during post-fabrication, increased disorder upon functionalization of the fullerene cage, and, in the case of C_{70} and its derivatives, cost prohibitive implementation, non-fullerene n-type materials are garnering increased attention (**Figure 5**).[82,83] Both small-molecule and polymer non-fullerene acceptors have been reported, with the choice of appropriate material depending on the optical gap of the electron donor material.[82] For example, a weaker electron acceptor, compared to a fullerene, can perform well when paired with a wide optical gap polymer such as P3HT due to reduced electron affinity offset. The opposite also holds true, wherein a low gap donor must be paired with a very strong electron acceptor to promote electron transfer. Several types of non-fullerene acceptors have been synthesized and studied, among which perylene diimide (PDI) and naphthalene diimide (NDI) oligomers and polymers have received the most attention.[84–87] PDI-based monomers have been shown to exhibit wide absorption bands, electron mobilities up to 1 $cm^2\ V^{-1}\ s^{-1}$, and electron affinities around 4 eV, all appropriate materials properties.[84] The large planar π-conjugated core has the ability to form strong π–π interactions and leads to micrometer-sized crystallites in the solid state. While these large crystallites allow for efficient charge transport, the drawback is that they limit the donor-acceptor interfacial area and act as trapping sites, limiting exciton diffusion and long-range charge transport.

There have been several strategies to minimize PDI aggregation without compromising electron transport efficiency, including the introduction of specific alkyl chains on the nitrogens (imide functionalization), functionalization at the ortho and bay positions, linking two PDI units through N—N bonds, and the development of PDI oligomers. Via functionalization at the bay position, Nuckolls and co-workers have demonstrated BHJ OSCs with PCEs of 8.3% using poly[4,8-bis(5-(2-ethylhexyl)thiophen-2-yl)benzo[1,2-b;4,5-b']dithiophene-2,6-diyl-alt-(4-(2-ethylhexyl)-3-fluorothieno[3,4-b]thiophene)-2-carboxylate-2,6-diyl] (PTB7-Th) as the electron donor;[88] in this instance, functionalization results in a twisted conformation that reduces crystallinity and increases processability of the PDI oligomers. Excitons generated in both donor and acceptor are found to contribute to the photocurrent through efficient electron and hole transfer at the donor-acceptor interface, mediated by strong interactions between PDI and the electron donor due to the twisted PDI conformation. Another way of introducing twists along the PDI oligomer relies on inserting aromatic rings between the PDIs.[89] For example, incorporating a thienylene ring between two PDI units has been shown to produce domain sizes of ≈30 nm while the PDI monomer yields crystalline domains on the order of 100 nm.

Apart from PDI-based oligomers, several other non-fullerene acceptors have been developed.[90–93] Examples include: fluorinated pentacene derivatives,[94] arylene diimide small molecules,[95,96] arylene diimide polymers,[87,97] benzothiadiazole-based small-molecules and copolymers,[98–106] rhodanine small molecules,[82,107,108] and electron-poor fused aromatic ring species.[109–114] Polyera have developed Polyera ActivInk N2200,[87] a NDI-based polymer, that has resulted in all-polymer devices with PCEs up to 8.3% using the J51 donor, a benzodithiophene fluorinated-benzotriazole copolymer.[115,116] The indacenodithiophene-benzothiadiazole-3-ethyl-rhodanine (IDTBR) acceptors of McCulloch and co-workers have achieved PCEs up to 6.4% using P3HT as an electron donor;[108] here, the performance of this system has been attributed to the complementary absorption profiles of IDTBR and P3HT that allow for photogenerated charge carriers in either acceptor or donor. Using P3HT as a donor and either a triphenylamine-based small molecule or benzothiadiazole copolymer, Lin et al.[117] and Mori et al.,[103] respectively, have demonstrated V_{OC} values up to 1.26 V by engineering materials with low electron affinity.

3.3. Molecular Interactions Between Fullerenes and Small Molecules/Polymers

In this Section, we provide a first discussion of the nature of the molecular interactions between fullerenes and electron donors. The active layer of solution-processed OSCs is formed by dissolving the electron donor and acceptor components and casting the mixture into a film. As the solvent evaporates, the electron acceptor and donor materials form a blend with partial phase separation distributed throughout the film. The performance of OSCs largely depends on the resulting nano-scale morphology since the morphology directly impacts the electron transfer rates,[118] charge separation,[119,120] charge recombination,[118,121] and charge transport pathways. While outside the scope of the current Review, it is important to note that the mesoscale morphological details also play a key role in determining the charge transport properties and performance of OSC devices.[122,123] Aspects of mesoscale order such as the importance of domain size,[124–126] percolation pathways,[127–129] and donor-acceptor phase segregation[130–132] have been discussed elsewhere and we direct interested readers to these works.

Exploration and characterization of the purity and size of the phase-separated domains have received significant attention.[1,127,132–138] Recent experimental investigations have attempted to determine the energy landscape in the mixed and pure phases. For instance, McGehee and co-workers have demonstrated energy-level shifts in the polymer donor due to structural disorder and intermolecular interactions between polymer chains and fullerenes using a combination of cyclic voltammetry and ultraviolet photoelectron spectroscopy; these authors have underlined the implications of these shifts on OSC efficiency.[139] Since it has been found that there is little to no charge transfer between polymer and fullerene in the ground state, the energy level shifts observed when mixing the two components can be attributed primarily to intermolecular van der Waals interactions.[140] On the other hand, the efficiency of photo-induced charge transfer between polymer and fullerene depends not only on the overall bulk morphology, but also on whether the polymer can accommodate the fullerene in close proximity to its backbone.[141,142]

As mentioned earlier, the solubility and processibility of the conjugated polymers from organic solvents is generally improved by attaching alkyl side-chains. It must be borne in mind that these side-chains can significantly alter the optical gaps, π–π stacking interactions, miscibility with fullerenes, and thin-film order. For instance, in the case of poly-benzodithiophene-thienothiophene (PTB)-based polymers (alternating benzodithiophene (BDT) and thienothiophene (TT) units), shorter π–π stacking distances have been observed when the BDT units are functionalized by two linear chains rather than two branched side-chains. Branched side-chains are also found to impact the thin-film structural ordering and the preferential orientation of the polymer backbones relative to the substrate, for example, in the case of poly-benzo[1,2-b:4,5-b']dithiophene–thieno[3,4-c]pyrrole-4,6-dione (PBDTTDP).[47]

A recent study by Graham et al. has highlighted that a priori minor changes in the structure and position of the alkyl side-chains of PBDTTPD can significantly affect the efficiency of the solar cells based on these polymers. For instance, when the thieno[3,4-c]pyrrole-4,6-dione (TPD) moieties carry (sterically accessible) linear alkyl side-chains and the benzodithiophene (BDT) moieties (more sterically hindered) branched side-chains, which implies that the $PC_{61}BM$ molecules are expected to locate preferentially around the TPD units of the polymer chain, the resulting system yields power conversion efficiencies up to ca. 8% and open-circuit voltages up to 1 V. On the other hand, for the same conjugated polymer backbone, much lower power efficiencies are observed if it is TPD that carries branched side-chains and BDT linear side-chains.[143] That it is better for the fullerenes to bind preferentially around the electron-rich moiety of the polymer backbone has been observed in a number of other instances. This trend is consistent with the transient spectroscopy data of Laquai and co-workers, which indicate that a

PBDTTPD polymer with branched side-chains on the electron-rich moieties and linear side-chain on the electron-poor moieties exhibits lower geminate and non-geminate charge-carrier recombination losses compared to the corresponding polymer with only linear side-chains.[144] In contrast, McCulloch and co-workers[145] have found that a copolymer consisting of thiophene flanked by an electron-poor 2,1,3-benzothiadiazole-5,6-dicarboxylic imide (BTI) segment carrying branched alkyl chains and an electron-rich benzo[1,2-b:3,4-b:5,6-d]trithiophene (BTT) segment leads to high power conversion efficiencies, up to 8.3%. In this case, it can be expected, however, that the electron-poor moiety, due to its larger size, is still able to interact with PCBM even when it carries branched side-chains. While more work is clearly desirable to better understand the relationship between the polymer-fullerene interactions, morphology, and PCE, probing such weak interactions and intermolecular arrangements between the polymer chains and the fullerenes in BHJs at the molecular scale remains a very challenging experimental proposition. Thus, the insights provided by computational studies could be extremely useful.

In this context, Ravva et al. have recently used long-range corrected density functional theory calculations to evaluate the binding between a long PBDTTPD oligomer and C_{60}. In the absence of any side-chains along the backbone, the C_{60} molecules prefer to bind through face-on configurations, which maximizes π–π interactions, and importantly, with little preference as to a specific position along the backbone.[146] The calculated binding energies per C_{60} are substantial, on the order of 12–15 kcal/mol. Thus, an interesting implication of these results in that eventually it is the polymer side-chains and the fullerene functional groups that dictate the preferential locations of the fullerene cages on top of the backbone. This conclusion is confirmed by the molecular dynamics simulations of Wang et al.[147] These authors have provided a detailed description of the impact that the nature and location of side-chains and functional groups have on the polymer-fullerene packing. They find that in general linear side-chains tend to extend away from the polymer backbone, while the bulkier branched side-chains tend to remain closer to the backbone. Thus, moieties carrying linear chains will have more room to accommodate fullerene molecules than those with branched side-chains. Their simulations on PBDTTPD-$PC_{61}BM$ confirm that the probability of finding $PC_{61}BM$ close to the TPD [BDT] moiety increases [decreases] when the TPD units carry branched side-chains compared to all linear side-chains.

4. Intermolecular Interactions and Processes in OSCs

4.1. Polarization Energy

The fact that organic electronic materials consist of a collection of non-bonded molecules or chain segments that interact via weak intermolecular interactions, inherently leads to significant structural disorder at room temperature; as a result, charge carriers are either strongly localized or weakly delocalized over just a few molecules or chain repeat units.[57,148–152] Intermolecular interactions also act to stabilize (photogenerated or injected) charges in the bulk material as compared to the gas phase, with the amount of stabilization directly related to the nature of the environment. In common organic electronic materials, this stabilization causes a reduction of the ionization energy (IE) and an increase of the electron affinity (EA) (**Figure 6**) on the order of an eV (**Table 1**);[153,154] it corresponds to the electronic polarization energy, defined by Lyons[150,155] as:

$$|P_+| = IE_{\text{solid-state}} - IE_{\text{gas-phase}} \quad (1)$$

$$|P_-| = EA_{\text{solid-state}} - EA_{\text{gas-phase}} \quad (2)$$

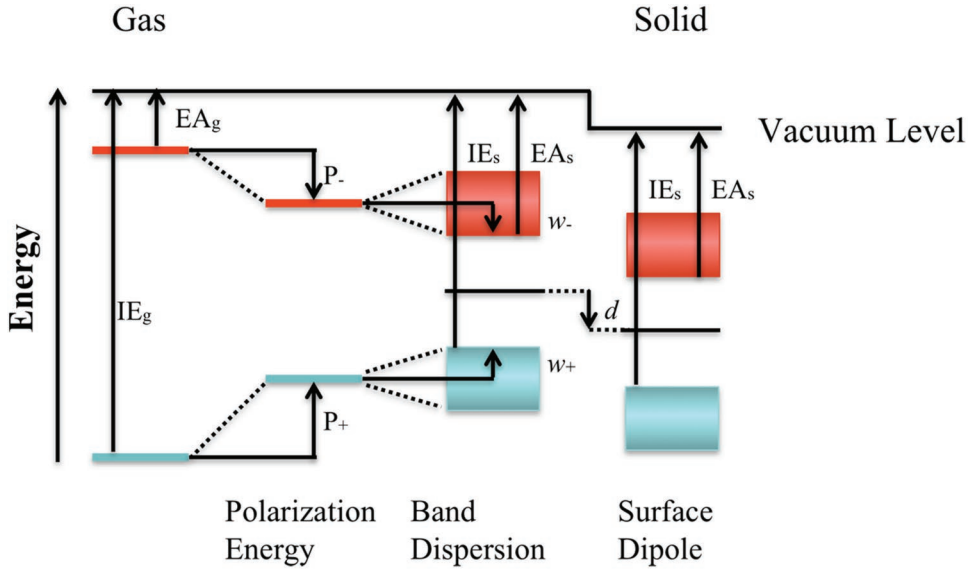

Figure 6. Energy level diagram in organic materials as the system evolves from the gas phase to the solid state. IE and EA represent the ionization energy and electron affinity, respectively. $P_{\pm}$ is the electronic polarization energy, w is the contribution from band dispersion, and d is the surface dipole that accounts for the orientation dependence of the IE and EA. Adapted with permission.[156] Copyright 2015, American Physical Society.

Table 1. Experimental polarization energies due to a positive (P_+) or negative (P_-) charge and polarization asymmetry for common organic electronic materials. All units in eV.

(eV)	$\|P_+\|$	$\|P_-\|$	$\|P_+ - P_-\|$
Benzene[a]	1.6	–	–
Naphthalene[b]	1.72	1.10	0.62
Anthracene[b]	1.65	1.09	0.56
Tetracene[c,d]	1.63	0.92	0.71
Pentacene[b]	1.63	1.12	0.55
Fullerene (C_{60})[e,f]	1.1–1.4	1.4–1.6	0.0–0.5
Perylene[a]	1.7	–	–
Rubrene[a]	1.1	–	–
Tetracyanoquinodimethane (TCNQ)[a]	2.1	–	–
Tetracyanonaphthoquinodimethane (TNAP)[a]	2.5	–	–

[a]Ref. [153], [b]Ref. [154], [c]Ref. [256], [d]Ref. [257], [e]Ref. [258], [f]Ref. [259].

Here, the polarization energy due to a positive [negative] charge, P_+[P_-], is the difference between the solid-state and gas-phase ionization energies [electron affinities]. Note that the IE [EA] of a specific donor [acceptor] site is referred to, in physics terminology, as the site energy. In what follows, we use the absolute value of the polarization energy as it is always stabilizing. As highlighted by Yoshida et al.,[156] effects from band dispersion and surface dipole must also be accounted for to accurately describe the polarization energy in organic electronic materials. Lattice and nuclear relaxations that occur at longer time scales than the electronic polarization also contribute some amount to the electronic polarization energy, generally estimated to be on the order of 0.1 eV.[150]

Polarization energy impacts a number of processes in organic electronic devices. Of focus here is the role of polarization on the charge separation and charge transport processes in OSCs. In the following discussion, we illustrate that even small changes to the electrostatic environment in the bulk donor and acceptor materials and at the donor-acceptor interface can cause changes in the polarization energy of several tenths of an eV.

4.1.1. Methods to Calculate Polarization Energy

Several methodologies have been developed for the calculation of the electronic polarization energy in organic molecular crystals. The methods range from simple isotropic functions that rely on experimentally obtainable data, to electrostatic models where each atom in the crystal is represented by multipole and polarizability matrices, and to hybrid quantum-mechanical/molecular-mechanical models that combine a quantum mechanical treatment with simple electrostatic interactions. In the Sections to follow, we briefly cover the most common models, taking molecular crystals as representative examples (we point the readers interested in more thorough discussions to the recent review by Beljonne and co-workers).[157]

Cavity in a dielectric medium: The simplest model to determine the polarization energy of a material is based on classical electrostatic theory, i.e., the Born model,[158] where the polarization energy relates to the stabilization of a point charge in a spherical cavity embedded in an isotropic polarizable medium:

$$P = \left(e^2/2\rho\right)\left(1-1/\varepsilon\right) \tag{3}$$

Here, ρ denotes the radius of the cavity and ε, the dielectric constant. This model was highlighted by Sato et al.,[153] who also proposed a modified version since ρ is generally difficult to determine:

$$P = 8.25e^2\bar{\alpha}\left(Z/V\right)^{4/3} \tag{4}$$

Here, in the context of a molecular crystal, $\bar{\alpha}$ represents the average molecular polarizability; Z, the number of molecules per unit cell; and V, the volume of the unit cell. Note that this model assumes an isotropic polarizability of the molecular systems. However, this is often not the case in organic π-conjugated systems as they are often significantly more polarizable along one axis due to their conjugated, elongated nature.[159] The unsubstituted fullerenes represent a notable exception since they have isotropic or nearly isotropic linear polarizability due to symmetry.[160,161]

Electrostatic models: Of the models that explicitly include terms for static (i.e., permanent multipole) and dynamic (i.e., induced dipole) electrostatic interactions, microelectrostatic models offer the flexibility to be as simple or complex as is desirable. For these models, the polarization energy is calculated by determining the static and dynamic intermolecular interactions in the presence and absence of an excess charge (i.e., the response of the system to an electric field) and represents the difference in energy between these two pictures. Here, the permanent multipole and linear polarizability tensors are distributed across an arbitrary number of points representative of the molecular system.

Early models[162] treated the molecules in a system as single polarizable points and calculated the interaction energy between an ion and the dipoles that it induces; the induced dipoles were not considered to interact with each other, resulting in, sometimes, poor agreement with experimental results. As microelectrostatic models became more complex, the induced-dipole interactions were treated self-consistently,[150,163] and molecules were represented by more than one point,[164] increasing agreement with experiment as the three-dimensional shape of the molecules is better reproduced.

More recently, two electrostatics models have been increasingly exploited in the literature: (i) the microelectrostatic model of Heremans and co-workers[10,165–167] and (ii) the AMOEBA force field-based model of Brédas and co-workers.[168] These models, while conceptually similar, differ in how they describe the molecular multipoles and the molecular polarizabilities. The Heremans microelectrostatic model divides the molecular quadrupole across a number of submolecular points such that each point is equivalent and recreates the molecular quadrupole in an additive fashion; the linear polarizability tensor is similarly divided across submolecular points and treated in an additive fashion. The AMOEBA-based model uses an atom-centered approach where each atom has charge, dipole, and quadrupole tensors from a distributed multipole analysis that

recreates the molecular electrostatic potential; the Thole model is used for the polarizability with atom-centered isotropic polarizabilities recreating the anisotropic molecular polarizability. Typically, these differing treatments result in only quantitative differences, although these actually depend on how the molecular multipoles and polarizabilities are partitioned.

Charge redistribution models: The charge redistribution models are based on a methodology originally proposed by Stone,[169,170] wherein molecules are divided into sub-regions that are individually polarizable. This model extends beyond the microelectrostatic models by allowing charges to redistribute in response to the electric field. Thus, while the overall charge of a given molecule remains unchanged, the net partial charges and multipoles at the various sites within a molecule evolve in response to the environment. Here, the charge flow is in the direction of the bonds; thus, polarization of the systems perpendicular to the bonds is not represented well.

There are two prominent charge redistribution models: (i) the model of Tsiper and Soos;[171,172] and (ii) the charge response kernel of Morita and Kato.[173–176] While very similar, these two models differ in how they treat polarization perpendicular to the direction of the bonds, which is poorly accounted for by the charge flow. In the former model, this is accomplished through assigning atomic polarizabilities, while in the latter polarizable auxiliary sites are used to capture this effect.

Quantum mechanical models: There have been a number of quantum mechanical approaches proposed for the evaluation of polarization energy.[11,177–183] These methodologies range from hybrid quantum-mechanical/molecular-mechanical (QM/MM) treatments that represent the bulk of the system as a polarizable field of point charges and the area of interest (the molecular ion) quantum mechanically, to constrained density functional theory (CDFT) methodologies that restrict a charge to a predefined region.

Given the wide range of models, we briefly focus here on just two: on one hand, the hybrid QM/MM model of Norton et al.[177] and, on the other hand, the fully quantum-mechanical treatment of Castet et al.[182] that restricts charges to individual molecules and calculates, self-consistently, the response of each molecular system in the bulk to the presence of an excess charge. These two approaches provide good examples of the different approaches to solving the electronic polarization problem. The hybrid QM/MM model has the advantage of being computationally inexpensive as only the charged species is treated at the QM level (typically this is done at the DFT level) while the bulk is treated at the MM level via force fields (e.g., UFF).[184] Within this model, the bulk is explicitly treated as a field of polarizable point charges that react to the presence of the QM region and that in turn influence the MM region; thus, this requires a self-consistent treatment. The downside to such an approach is that the electrostatic potentials of nonpolar molecules is not accurately reproduced, leading to qualitative errors in higher-order multipole (i.e., greater than dipole) interactions with the charged QM region. The fully quantum mechanical valence bond Hartree-Fock (VBHF) model of Castet et al.[182] surmounts this deficiency by treating every molecule in the system quantum mechanically. To overcome the computational cost that comes with such a treatment, each molecule is treated at the semiempirical level (using the neglect of diatomic differential overlap, NDDO, Hamiltonian) and the charge of each molecule is predefined. In this manner, the energy of the system is solved in a self-consistent fashion where each molecule feels the electric field generated by all surrounding molecules. Similar methodologies that utilize constrained density functional theory to provide a better description of the molecular polarizability have also been used to great success.[183]

4.1.2. Influence of Intermolecular Interactions on Polarization Energy

Since the seminal experimental work of Sato et al.,[153] the polarization energies of bulk organic π-conjugated molecular materials had largely assumed to be similar, approximately 1.7 eV. However, as work continued to better describe this phenomenon, it became increasingly clear that this is not necessarily the case. The work of Koch and co-workers[185–187] has clearly demonstrated that: (i) the molecular orientation has a profound impact on the ionization energy, with the IE of pentacene varying by some 0.55 eV (**Figure 7**); (ii) by changing the sign of molecular quadrupole components, e.g., via perfluorination, the IE of a material such as pentacene can be shifted by nearly 2 eV.[186] Indeed, different molecular orientations or the sign of molecular quadrupoles impacts the molecular interactions significantly. To better understand how the local electrostatic environment determines the ionization energies of

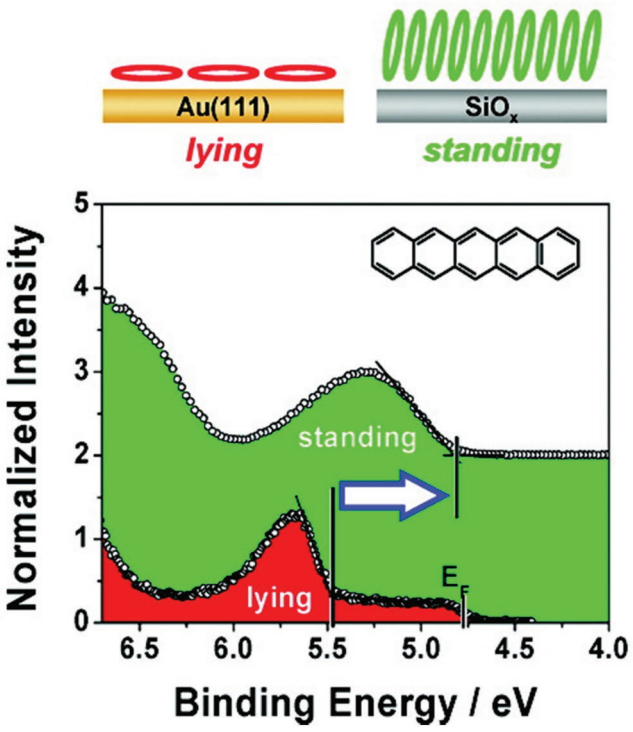

Figure 7. Experimental ultraviolet photoemission spectra of a monolayer of pentacene lying face-on to a Au(111) surface (red) and a thin film of pentacene standing edge-on to a silicon oxide surface (green). The energy reference is the vacuum level directly above the sample. The Fermi level, E_F, is noted for the Au substrate. Reproduced with permission.[187] Copyright 2010, American Chemical Society.

organic electronic materials, and thus the polarization energy, we first discuss bulk materials before moving on to organic-vacuum interfaces and organic-organic interfaces.

As stated above, electronic polarization in many organic π-conjugated molecular crystals is approximately 1.7 eV. However, even in materials that are structurally similar the electrostatic environment can be substantially different, due to packing variations[188] or the amount of structural disorder in the material.[57] Ryno et al. have investigated a series of oligoacenes and their 6,13-bis(2-(tri-isopropylsilyl)ethynyl (TIPS) substituted derivatives. Although pentacene and TIPS-pentacene are electronically similar (i.e., the molecular quadrupoles and linear polarizabilities are similar), the manner in which they pack is significantly different. Pentacene packs in a herringbone motif and TIPS-pentacene in a brickwork motif, which results in markedly different intermolecular interactions; specifically, the quadrupole-quadrupole interactions are stabilizing in pentacene, while they are destabilizing in TIPS-pentacene. As a result, there occurs a large reduction in the calculated polarization energy of TIPS-pentacene (P_+, 0.59 eV; P_-, 0.69 eV) compared to pentacene (P_+, 1.02 eV; P_-, 0.79 eV). Additionally, the polarization asymmetry (i.e., the difference between P_+ and P_-) decreases from 0.23 eV in pentacene to 0.10 eV in TIPS-pentacene. In a subsequent study, Ryno et al. investigated the effect of packing density for a given packing motif (herringbone), comparing tetracene and rubrene; they observed strong dependence of P_+ on the intralayer (*a*/*b*-plane) packing density and an order-of-magnitude smaller impact on polarization energy for the interlayer (*c*-axis) density.[189]

Even in the case of crystalline materials, defects can be present in the form of grain boundaries between crystallites, which act to impede charge transport. Verlaak and Heremans,[10] through modeling four idealized types of grain boundaries in pentacene showed that sites next to the boundaries can act as either intrinsic barriers or trapping sites, depending on whether the space between grains is filled or not, and inhibit efficient charge transport. These authors showed that for both voids and filled grain boundaries, charge-quadrupole interactions are responsible for the resulting traps or barriers, with both spanning the range from 0.1 eV to 0.4 eV. We note that this investigation used rigid crystals for the modeling of the grains; thus, energetic disorder due to molecular motions comes as an additional contribution.

In a recent investigation on a series of fullerenes, D'Avino et al.[57] find that although the polarization energies of these systems are similar, each possesses differing amounts of energetic disorder resulting in various polarization energy distributions (**Figure 8**). For the fullerene derivatives investigated, the polarization energy distributions centered around 0.9–1.0 eV; however, due to the different electrostatic interactions present in C_{60} (rank 6) versus $PC_{61}BM$ or $PC_{71}BM$ (dipolar), the standard deviations covered a large range: Crystalline C_{60} has a narrow distribution with $\sigma = 0.005$ eV; crystalline $PC_{61}BM$ is more disordered due to the dipolar interactions with $\sigma = 0.085$ eV; and amorphous $PC_{71}BM$ is the most disordered with $\sigma = 0.160$ eV. Thus, the variations in intermolecular interactions cause the standard deviations of the polarization energy distributions to change by a factor of ca. 30.

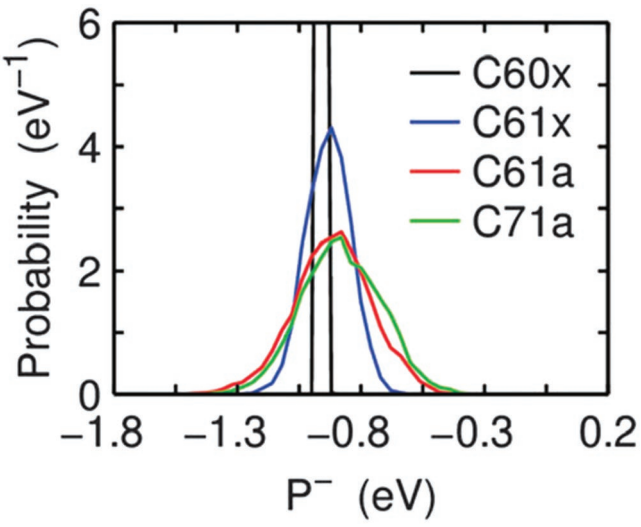

Figure 8. Probability distribution of polarization energies due to a negative charge carrier, P_-. C60x has a maximum probability of 25 eV^{-1}. Reproduced with permission.[57] Copyright 2016, Royal Society of Chemistry.

We now move our attention away from the bulk materials to consider interfaces. Salaneck[190] reported that the ionization energy at an anthracene surface was some 0.3 eV larger than in the bulk. There have been numerous investigations that have probed the organic-vacuum interface to determine the origin of this reduced polarization energy at the surface compared to the bulk. Tsiper and Soos[191] and Ryno et al.[189] discussed the pentacene and tetracene surfaces, respectively. They report that, for a hole, the polarization energy at the surface is reduced by approximately 0.1 eV with respect to the bulk; interestingly, this net P_+ reduction at the surface is the result of two competing contributions, a (larger) reduction in stabilization related to induced interactions and an increased stabilization related to static interactions. We note that, Gorczak et al.[192] have reported that there is no change in the magnitude of the polarization energy between the pentacene(001) surface and the bulk, but describe similar trends for the induced and static interactions as Ryno et al. Thus, while there is general consensus that the intermolecular interactions at the surface differ from the bulk, the net effect on the surface polarization is still a matter of debate.

In OSCs, the processes of exciton dissociation and formation of charge transfer states occur at organic-organic interfaces. As has been underscored by a number of authors, the electrostatic environment at these heterojunctions is clearly very different from that of the surface.[119,123,165,166,192–197] In a recent investigation, Ryno et al.[196] have shown that, in the case of the pentacene(001)/C_{60} interface, each donor and acceptor site has in fact a unique electrostatic environment. Polarization energies vary not only from site-to-site but also change significantly as a function of time, due to molecular vibrations and motions. The polarization energies for pentacene molecules along the interface range from about 0.9 eV to 1.1 eV, while the polarization energies for the interfacial C_{60} molecules range from less than 0.75 eV to 0.85 eV. The reason for these distributions in polarization is found in the variations in charge-quadrupole and induced-dipole interactions amongst molecular sites (**Figure 9**).

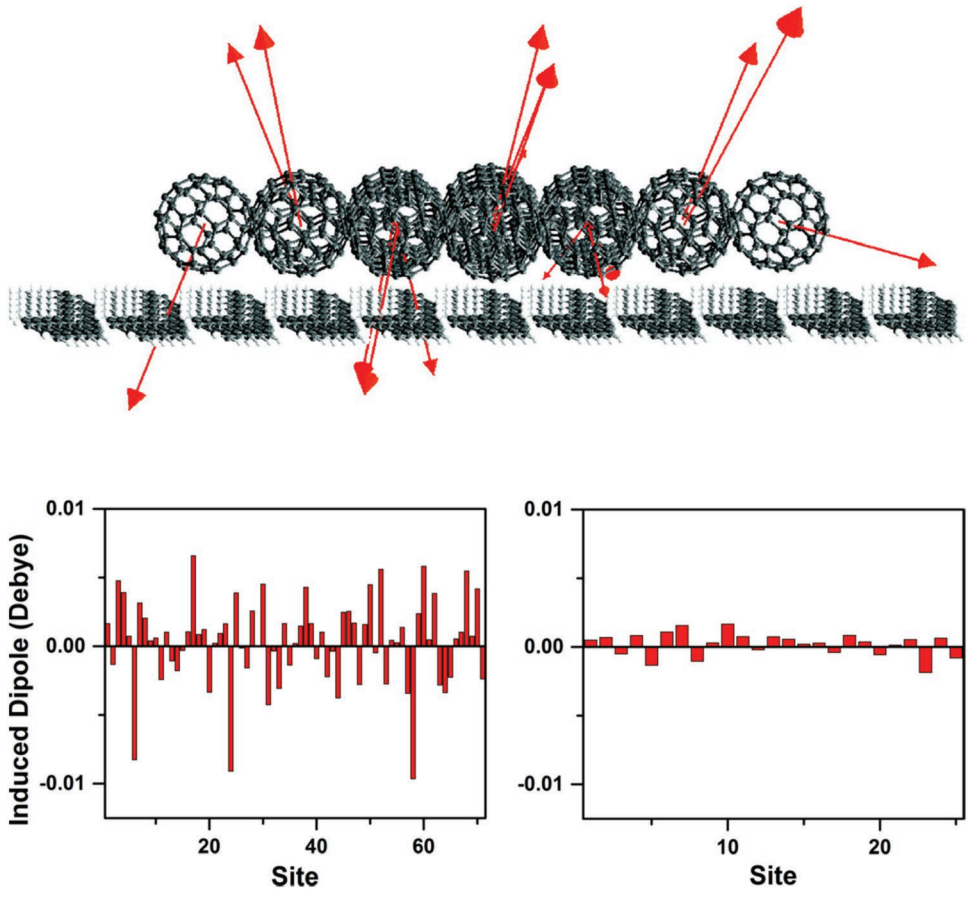

Figure 9. Top: Induced-dipole moment vectors of C_{60} molecules at a pentacene/C_{60} heterojunction. Adapted with permission.[166] Copyright 2010, American Chemical Society. Bottom: The *z*-component of the induced dipole on pentacene (left) and C_{60} (right) molecules at a pentacene(001)/C_{60} heterojunction. Adapted with permission.[196] Copyright 2016, American Chemical Society.

This feature has also been highlighted by Linares et al.[166] for the pentacene(01-1)/C_{60} interface; these authors pointed out that not only does the magnitude of the induced dipoles change from C_{60} to C_{60} molecule along the interface, but its directionality as well. As will be discussed later, the nature of the intermolecular interactions among organic molecules at the heterojunction interface can be tuned to promote charge separation in OSCs.

Theoretical investigations focusing on polarization in polymeric materials are much more infrequent than for small molecules. This limitation is primarily due to the difficulty of describing such extended systems in a computationally feasible manner. The recent works of Beljonne and co-workers have attempted to tackle this problem using the poly(3-hexyl)-thiophene (P3HT) and $PC_{61}BM$ or C_{60} model systems.[198] They note overall smaller polarization energies but broader distributions at the P3HT/$PC_{61}BM$ interface than in a P3HT/C_{60} system. Similar to the investigation of D'Avino et al.,[57] the authors highlight increased energetic disorder at $PC_{61}BM$ interfaces than at C_{60} interfaces, due to the permanent dipole present in $PC_{61}BM$; such disorder will come into play when discussing charge separation. Each of the works discussed above underlines that a proper account of the intermolecular interactions is necessary to accurately account for the effects of the electrostatic environment.

4.2. Delocalization

It is important to note that the majority of the works we have discussed so far have been conducted in context of charge carriers being localized. This approximation allows for the use of computationally inexpensive methodologies such as microelectrostatics, valence-bond/Hartree-Fock, or constrained-DFT to describe molecular clusters. However, it has been pointed out that delocalization effects can be of importance to describing charge separation and the nature of the charge transfer states.[121,199–204] Until recently, theoretical work devoted to understanding delocalization in organic electronic materials had been limited. In the realm of small molecules, Yang et al.[148] have used long-range corrected DFT to study the impact of delocalization on the charge transfer (CT) state energy. Upon increasing the number of pentacene molecules in a model pentacene/C_{60} interface, there occurs a 0.3 eV reduction in the CT state energy for face-on configurations, and a 0.8 eV reduction for the edge-on configurations. These authors thus draw attention to the importance of delocalization while at the same time highlighting the limited size of systems that can be investigated using common electronic structure methodologies.

Beljonne and co-workers have proposed, in a number of works,[57,121,195,198,202] electron and hole delocalization to be a

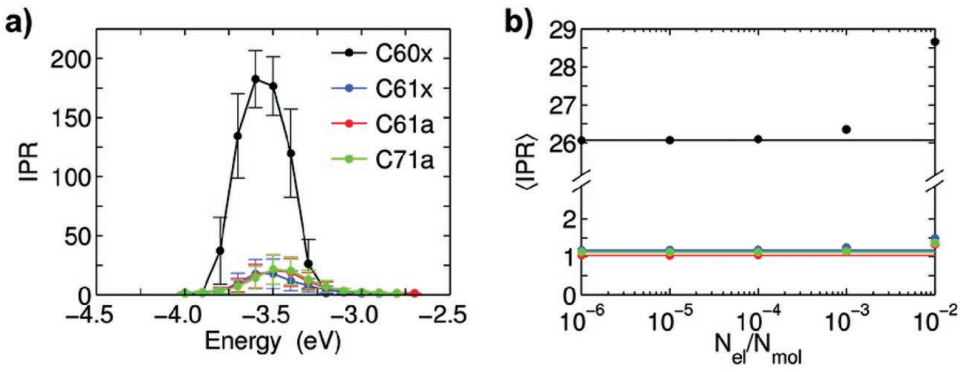

Figure 10. a) Distribution of the inverse participation ratio (IPR), which quantifies the number of molecules over which eigenstates are delocalized. b) Thermal averages of the IPR at 300 K as a function of the charge carrier density, as calculated with Fermi-Dirac statistics. Straight lines are the density-independent Boltzmann thermal averages. Dots represent the average values and error bars represent the standard deviations. C60x is crystalline C_{60}, C61x is crystalline $PC_{61}BM$, C61a is amorphous $PC_{61}BM$, and C71a is amorphous $PC_{71}BM$. Reproduced with permission.[57] Copyright 2016, Royal Society of Chemistry.

key factor in the dissociation of the exciton at donor-acceptor interfaces. In crystalline C_{60}, they estimate electrons to delocalize over about 26 molecular sites, in agreement with some experimental observations;[205] however, the delocalization of an electron in functionalized PCBM is much more limited due to energetic disorder related to the permanent dipole moment (**Figure 10**). This comes in contrast to Cheung and Troisi[206] who suggested delocalization of the electron across 40 molecules in $PC_{61}BM$, although this result is probably affected by the neglect of site energy differences among the fullerene molecules. Moreover, both D'Avino[57] and Street[207] and their co-workers point to decreasing delocalization with increasing fullerene size, which suggests that reduced delocalization is due to increasing energetic disorder in the larger fullerenes.

Savoie et al.[204] have taken a different approach and investigated the effects of fullerene cluster size and dimensionality on the delocalization of states within fullerene acceptor materials. They obtain that efficient free charge carrier generation results from good overlap of charge-separated states in the fullerene acceptor and excited states in a polymer donor. Moreover, they suggest that the ability of fullerenes to form extended three-dimensional networks aids in the formation of such delocalized states and eventually charge separation; on the other hand, polymer non-fullerene acceptors, due to their bulky side-chains, might inhibit the formation of these delocalized states.

Turning to delocalization in polymer donor materials, Beljonne,[198] Burghardt,[199,200,208] and Thompson[207] and their co-workers have investigated charge carrier delocalization in derivatives of polythiophene mixed with PCBMs of various sizes. For crystalline polymer domains, they each suggest delocalization on the order of ten molecular units, with delocalization being beneficial to charge separation. Tamura and Burghardt[200] note a decreased delocalization of the hole electronic states at the donor-acceptor interface than in the pure donor material because of increased energetic disorder. Additionally, Castet et al. have shown in the $P3HT/PC_{61}BM$ system that high-lying CT states, wherein the hole is delocalized over several polymer repeat units, become accessible due to the polarization effects of the local environment;[195] these authors suggest that these delocalized states may not only assist in charge separation, but also act to reduce charge recombination.[121] Thus, these works highlight that the intermolecular interactions dictate the amount of delocalization in these complex systems, an effect that needs to be considered even though its description is computationally challenging.

4.3. Charge Transfer States

When an exciton appears at the donor-fullerene interface, an excited electron can jump from the electron donor to the fullerene and form a charge transfer (CT) state, from which separation of electron and hole generates free charge carriers. The discussion in the previous Sections has illustrated that intermolecular interactions greatly impact the ionization energies and electron affinities of donors and acceptors, and that the interactions between adjacent donors and acceptors can be modified by the orientation of the respective moieties or their environment. The energy of the lowest-lying CT state (CT_1) can be approximated as:[209]

$$E(CT_1) = IE_D - EA_A + E_{Coul}(D:A) \quad (5)$$

Here, IE_D is the ionization energy of the electron donor, EA_A is the electron affinity of the electron acceptor, and $E_{Coul}(D:A)$ is the Coulombic attraction between the hole on the donor and the electron on the acceptor (we recall that the first two terms are positive quantities while the third one is negative). Thus, the CT state energy is expected to be extremely sensitive to the molecular-scale interactions between donor and acceptor.

Because of its strong dependence on molecular interactions, the CT state energy can span a broad range by varying molecular structure, packing, and degree of aggregation. Making again reference to the work of Yang et al. on model pentacene/C_{60} complexes using long-range corrected density functional theory, it was shown that there occurs an enhancement of hole delocalization as a function of increasing the number of pentacene molecules in the complex, which acts to decrease the energy of the CT state; this results from an increase in the distance between the centers of the electron and hole distributions.[148] Furthermore, by rotating the pentacenes from a face-on orientation to an

edge-on orientation, thereby changing the sign of the interacting quadrupoles and increasing the distance between hole and electron, there is a nearly 0.5 eV increase in the CT state energy.[148]

The influence of intermolecular interactions extends past simply determining the CT state energy, as they play a key role in assessing the open-circuit voltage (V_{OC}) and determining to which sites the CT state moves along the donor-acceptor interface during CT state energy transfer.[21,210] In the case of the 4,4',4''-tris(phenyl(*m*-tolyl)amino)triphenylamine:tris(2,4,6-trimethyl-3-(pyridine-3-yl)phenyl)borane system, Deotare et al.[211] have experimentally observed CT states to migrate along the donor-acceptor interface for distances between 5–10 nm, and have corroborated these findings with Kinetic Monte Carlo simulations. Their simulations point to the movement of the electron-hole pair as proceeding in stretch-pull fashion along the interface, whereby one charge carrier first moves and the other follows. The interfacial energetic disorder, estimated to be on the order of 100 meV or more, has also a negative impact on V_{OC}.[21,212] Using a numerical model, McGehee and co-workers have demonstrated that decreasing the energetic disorder from 100 meV to 50 meV can increase V_{OC} by up to 120 mV.[21] Furthermore, Coropceanu and co-workers have separated this disorder into static and dynamic components, allowing for these contributions to be independently considered.[81,213]

4.3.1. Theoretical Determination of the CT-State Energies and Characteristics

The exact determination of the nature of the CT states, be them more delocalized higher-energy states or more localized lower-energy states, has proven to be difficult and is currently the focus of many investigations in the theoretical community.[209,214–217] Linear-response TD-DFT has been a popular choice for the determination of excited-state properties due to its reasonable computational cost.[218] Due to their tendency to promote excessive delocalization, common hybrid functionals (e.g., B3LYP and PBE0) strongly underestimate the CT excitation energies.[219] The use of non-empirically tuned long-range corrected functionals (that significantly reduce the electron self-interaction error), such as BNL,[209] ωB97X,[220] and LC-ωPBE,[221] suppresses this overdelocalization and provides reliable estimates of the low-lying CT state energies. However, describing the higher-lying CT excitations remains more difficult.[216,218] To address this issue, recent studies from the groups of Blasé[217,222,223] and Rohlfing[214,224,225] have employed many-body Green's function theory by combining the GW approximation and the Bethe-Salpeter equation (BSE) to investigate the optical excitations in two donor-acceptor model complexes, anthracene-tetracyanoethylene[226] and fullerene -oligomer donors systems.[214,215,225] While such GW-BSE calculations give good agreement with high-level ab initio methods (e.g., CASPT2),[222] their computational cost still limits their implementation.[215]

4.4. Charge Separation

Several models have been proposed as possible pathways to overcome the barrier to charge separation once an exciton appears at the donor-acceptor interface. It has been suggested early on that hot CT states, that form after the initial photoexcitation and prior to relaxation to the lowest-energy CT state, might play a role in charge separation, by providing enough energy for the charges to separate prior to relaxation to the bottom of the CT state distribution. However, the work of Baldo and co-workers and, in particular, of Vandewal and co-workers, has demonstrated that the lower CT states are key intermediates to the separation process.[211,227] McGehee and co-workers[21] have recently proposed that the lower CT states are in fact in equilibrium with the charge separated (free carrier) states. Thus, it is of interest to examine the complex energetic landscape that occurs at the donor-acceptor interface and its impact on the terms appearing in Equation. (5).

We first discuss the work of Verlaak et al.[165] who used a model pentacene/C_{60} interface (wherein a slab of crystalline C_{60} was deposited onto a crystalline slab of pentacene) to determine how molecular orientations and local electrostatic environments influence the energy required for charge separation. Focusing on the pentacene(001) (edge-on) and pentacene(01–1) (face-on) surfaces, these authors showed that a hole-electron pair at the edge-on interface is 0.6 eV more stabilized than at the face-on interface. This increased stabilization translates to a 0.44 eV charge separation barrier for a hole and an electron at the edge-on interface and a 0.04 eV barrier at the face-on interface. The origin of this difference is related to the different orientations of the pentacene molecules, which changes the sign of the quadrupole interacting with C_{60}, and thus, the sign of the induced dipoles in C_{60}. While the face-on pentacenes are closer to the C_{60} molecules, and the charges have a larger Coulombic interaction (–1.11 eV for edge-on; –1.73 eV for face-on), the closer the hole and electron get, the more they appear as a neutral species. This results in a drastic reduction in the stabilization due to induced dipoles, which cuts the –1.19 eV induced-dipole stabilization for the edge-on system in half to –0.59 eV (**Table 2**).

In a follow-up investigation, Linares et al.,[166] and later Idé et al.,[119] demonstrated interfacial band bending as a function of pentacene orientation; moving away from face-on pentacene by rotating the pentacenes in 10° increments until an edge-on configuration is obtained, can result in HOMO/LUMO shifts of about 0.2 eV (**Figure 11**). In the face-on orientation, there is a large induced dipole on both pentacene and C_{60} that is oriented towards the C_{60}; as the angle of the pentacene plane increases, the induced dipole becomes smaller and eventually changes sign. This has the effect of destabilizing the hole and electron in the face-on orientation and stabilizing them in the edge-on orientation, which induces a larger charge separation barrier for edge-on pentacene.

Building upon the works of Idé et al.[119] and Verlaak et al.,[165] Yost and Van Voorhis showed how electrostatic interactions and dielectric differences at the interface influence the interfacial energy levels to create environments that can be more, or less favorable to charge separation (**Figure 12**).[228] Using QM/MM simulations that account for either a single hole or electron, they show how the HOMO and LUMO levels in donor and acceptor materials shift in response to the electrostatic environment. Taking rubrene and C_{60} as a model system, with dielectric values of 2.7 and 3.8, respectively, these authors find

Table 2. Interaction energies for an electron-hole pair near the interface and separated far from the interface for both the pentacene(001)/C_{60} and pentacene(01–1)/C_{60} interfaces. Hole (h) is on an interfacial pentacene and electron (e) is on an interfacial C_{60} for the bound pair. QID is the quadrupole-induced-dipole interaction energy. All units in eV. Reproduced with permission.[165] Copyright 2009, John Wiley and Sons.

		Electron-hole pair	Separated electron and hole
Pentacene(001)/C_{60}	Coulomb energy	−1.114	0
	Induced-dipole interaction	−1.188	−1.058(h) − 0.791(e)
	Quadrupole interaction	−0.415(h) − 0.119(e)	−0.310(h) + 0.004(e)
	QID interaction	+0.132(h) + 0.019(e)	−0.053(h) − 0.039(e)
	Total	−2.685	−2.247
Pentacene(01-1)/C_{60}	Coulomb energy	−1.732	0
	Induced-dipole interaction	−0.593	−1.052(h) − 0.792(e)
	Quadrupole interaction	+0.025(h) + 0.284(e)	-0.302(h) + 0.004(e)
	QID interaction	+0.053(h) − 0.128(e)	+0.043(h) + 0.044(e)
	Total	−2.091	−2.055

that the dielectric mismatch results in the HOMO/LUMO gap of rubrene becoming smaller near the interface (Figure 12a); this results from increased stabilization of both hole and electron. On the other hand, the HOMO and LUMO of C_{60} are destabilized, which results from overall reduced polarization energy. Thus, the 1.1 dielectric constant difference results in shifts of over 0.1 eV for each of the energy levels. To model the effects of changing multipole interactions, these authors use two model interfaces of 4-(dicyanomethylene)-1-methyl-6-(4-dimethylaminostyryl)-4H-pyran (DMC) with C_{60} (one with zero interface dipole and one with interface dipole pointed towards the C_{60} layer). In the system with no interfacial dipole, there occurs relatively little modification to the energy levels at the interface; however, in the presence of a strong interface dipole, there are marked shifts of up to 1.0 eV in the HOMO and LUMO levels of DMC and C_{60} (Figure 12c). In this case, the interface dipole creates a situation where both hole and electron preferentially move away from the interface; here, the HOMO [LUMO] level in DCM is destabilized [stabilized] at the interface while the HOMO [LUMO] level in C_{60} is stabilized [destabilized]. However, it should be borne in mind that the stabilization/destabilization of the HOMO/LUMO levels is dependent on the direction of the interface dipole.

Looking more closely at how molecular motions influence intermolecular interactions, Ryno et al.[196] and Poelking and Andrienko[197] have investigated the effect of disorder at the small-molecule donor-acceptor interface. Using a model pentacene(001)/C_{60} bi-layer interface, Ryno et al. employed molecular dynamics to observe how the charge separation barrier changed as a function of both time and position along the interface. These authors show that, in general, the IE of pentacene and EA of C_{60} are stabilized at the interface; however, the disorder results in distributions with widths of nearly 0.2 eV, and leads to charge separation barriers with widths of about 0.2 eV centered at about 0.75 eV (Figure 12). They note three primary pentacene/C_{60} configurations, two with pentacene directly beneath a C_{60} and one where pentacene is positioned between three C_{60} molecules. While the charge separation barrier shows little change over time for the first two configurations (up to 0.09eV), the third site shows much more drastic change, e.g., the charge separation barrier for a single site can change by 0.17 eV over a timespan of less than 10 ps. This large change in charge separation barrier leads to the suggestion that some mixing or disorder at the interface can be beneficial for charge separation, if specific configurations can be realized.

Poelking and Andrienko[197] and Fu et al.[229] have found that even at a bi-layer interface there are protrusions of donor into the acceptor and acceptor into the donor. Using molecular dynamics snapshots of a bilayer based on a dicyanovinyl-substituted thiophene derivative (D5M) and C_{60}, Poelking and

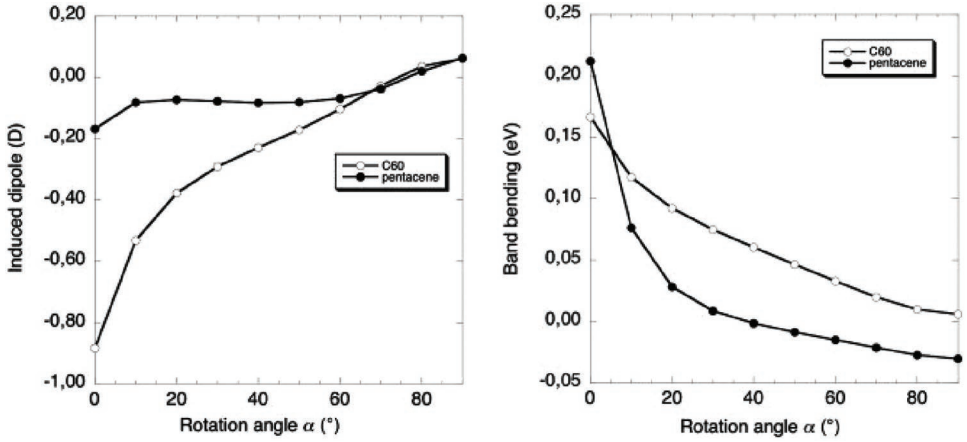

Figure 11. Left: Induced dipole of the interfacial pentacene and C_{60} in a 1-dimensional stack as a function of the rotation angle. 0° is face-on and 90° is edge-on. Negative values indicate an induced dipole oriented towards C_{60}. Right: Band bending of the interfacial pentacene and C_{60} in a 1-dimensional stack as a function of the rotation angle. Larger values for C_{60} indicate decreasing electron affinity, and larger values for pentacene indicate increasing ionization energy. Adapted with permission.[119] Copyright 2010, John Wiley and Sons.

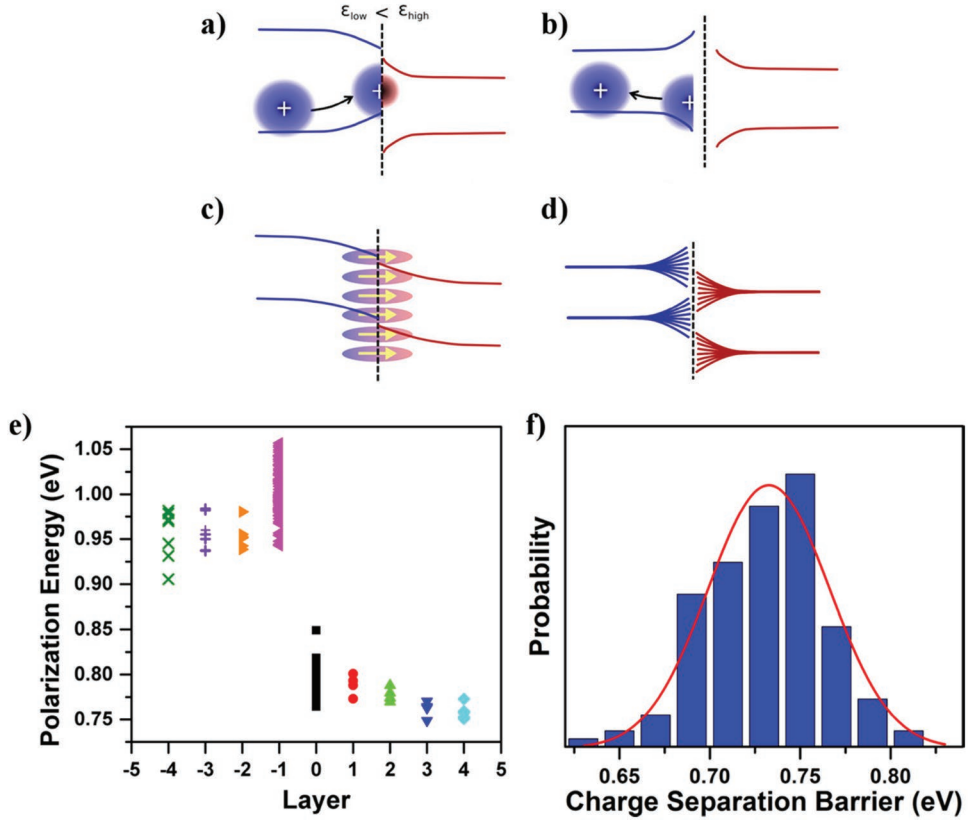

Figure 12. Top: Schematic representation of environmental effects on the band structure at the donor (blue) and acceptor (red) interfaces, including: a) a difference in dielectric constant, b) poor molecular packing (represented as the insertion of a vacuum layer), c) static multipole moments creating an electric field, and d) the effect of disorder at the interface. e) The polarization energy due to a hole or electron on the donor (layer < 0) or acceptor (layer ≥ 0) side of a pentacene(001)/C_{60} interface. f) Distribution of charge separation energies at a disordered pentacene(001)/C_{60} interface. Figures (a–d) are adapted with permission.[228] Copyright 2013, American Chemical Society. Figures (e–f) are adapted with permission.[196] Copyright 2016, American Chemical Society.

Andrienko find that as the orientations of the donor molecules change, and thus, as well the signs of the electrostatic interactions, hole and electron pairs may either be bound or separate: For face-on donor molecules in the protrusion at the interface, the intermolecular interactions favor charge separation as holes and electrons are destabilized, while the opposite occurs for the edge-on systems. Additionally, charge separation occurs preferentially when donor-acceptor pairs lie on either side of the plane of the interface, rather than along the direction of the interface; in some cases, the energetics at the interface can lead to unbound electron-hole pairs.

For polymer donor/fullerene acceptor systems, the concept of a localized charge carrier becomes more difficult to define since even when a hole is localized to a single polymer chain it may be delocalized over several repeat units. D'Avino et al. have attempted to tackle this issue in the limit of a charge localized to a single chain[198] and by allowing the hole and electron to delocalize across multiple molecules.[121] In the limit of localization along a single polymer chain, in this case P3HT in a bi-layer configuration with C_{60}, the charge separation barrier distribution from MD simulations is centered around approximately 0.25 eV with only 3% of electron-hole pairs likely to dissociate. However, when a P3HT/$PC_{61}BM$ bi-layer is considered, approximately 30% of electron-hole pairs are likely to dissociate, the reason being the energetic disorder coming from the dipole of $PC_{61}BM$. As discussed in Section 4.2, allowing holes and electrons to delocalize within the donor and acceptor materials, respectively, is expected to increase the possibility of hole-electron dissociation.

From Verlaak et al.'s[10] model using crystalline slabs of pentacene and C_{60} brought into close contact, to the investigation of Yost and Van Voorhis[228] into the effect of electrostatics on band bending, to the polymer:fullerene investigations of D'Avino et al.,[198] each of these works explores how intermolecular interactions impacts the charge separation process in OSC active layers. By controlling the multipole interactions among molecules, the polarizability of donor and acceptor moieties, and the disorder at the donor-acceptor interface, we can begin to apprehend how the energy required for charge separation can be tailored.

4.5. Charge Transport

Regardless of whether OSCs, organic light-emitting diodes, or organic field-effect transistors are being considered, the performance of these devices is limited by the efficiency by which charge carriers can be transported within the active layers.

There have been numerous exhaustive reviews on charge transport and the effects of molecular interactions on transport. As such, we direct interested readers to the reviews of Coropceanu et al.[9] and Gershenson et al.,[230] the books of Pope and Swenberg[152] and Silinsh and Capek,[231] and the book chapter of Li et al.[232] Here, we restrict ourselves to a discussion of Kinetic Monte Carlo (KMC) simulations, one of the methodologies used to model charge transport in OSC devices on the device scale while including information on the microscopic interactions; our objective is to illustrate how morphology influences transport, in particular in the case of fullerenes.

4.5.1. Brief Description of Kinetic Monte Carlo Simulations to Model Processes in OSCs

KMC simulations have proven to be a very useful tool for modeling OSC devices.[233–243] Simply put, KMC simulations allow for the description of the dynamic evolution of a given system composed of microscopic processes, i, that occur at some rate, k_i, over a given period of time. Thus, KMC simulations can be thought of as a theoretical experiment conducted under perfect, predefined conditions. Since the major microscopic processes in an OSC happen after photon absorption – exciton migration, exciton dissociation, charge transport, recombination, and charge collection at the electrodes – each has well-defined or parameterizable rates; these rates can be used as input for KMC simulations to understand the physics in OSC devices.[233] From these simulations, device properties such as current density, charge transport mobility, internal quantum efficiency (IQE), or external quantum efficiency (EQE) can be extracted.

Depending on the strength of the interactions between fullerene and electron-donor materials, varying degrees of phase separation can occur. Strong interactions result in well-mixed morphologies, while weaker interactions lead to increased phase separation. Such structural differences significantly impact the performance of the microscopic processes in OSCs. One of the primary advantages of KMC simulations over numerical modeling techniques, such as one-dimensional drift-diffusion simulations, is that specific characteristics of the morphology can be considered, which allows the investigation of relationships between the morphology and device performance.[244] Numerous KMC investigations have confirmed that morphology influences the fundamental processes taking place in OSCs. One early finding by Watkins et al.[233] is that excessive phase separation reduces the internal quantum efficiency, as it prevents excitons from reaching the donor-acceptor interface and increases the probability of excitons decaying before dissociation. However, in blended structures with large interfacial areas, excitons have increased probability of reaching the interface and dissociating. Thus, upon reaching the interface, the exciton may dissociate into free holes and electrons, recombine before separation (geminate recombination), or recombine after separation (nongeminate recombination), with morphology and intermolecular interactions determining the probability of each occurring. In their work, Marsh et al.,[234] using various system morphologies, have found that geminate recombination is generally more common than nongeminate recombination, because of the energy they consider as needed to initially separate the hole and electron. However, altering the electrostatic interactions at the interface, by changing molecular orientation as highlighted by Idé et al.,[119] or by changing the orientation of the interface relative to the direction of the electric field, can result in electric fields favorable to charge separation, while improving charge transport.[234,235]

Increased interfacial area has been calculated to lead to increased probability of charge recombination thereby, reducing performance.[233] Groves et al.[236] have shown, with the aid of drift-diffusion modeling, that changes in local carrier mobilities can result in significant differences in currents and overall device performance, due to increased bimolecular recombination rates. From such simulations that have focused on specific aspects of the whole OSC device, optimal performance has been suggested to be at an intermediate degree of phase separation, regardless of the actual blend morphology.[233,235,238]

4.5.2. KMC modeling of Charge Transport in Fullerenes

In combination with other techniques, KMC simulations can be used to investigate some of the microscopic processes in more detail. Here, we discuss KMC investigations of the charge transport properties of fullerenes and their derivatives.

Nelson and co-workers[245,246] have used molecular configurations from MD simulations as input into KMC modeling. Based on evaluated parameters such as the charge transfer integral and reorganization energy, KMC simulations can provide estimates of charge mobilities, which are found to be comparable to the experimental values. For disordered/amorphous C_{60}, the field-effect mobilities calculated by Kwiatkowski et al.[247] range from 2.4 to 4.4 $cm^2\ V^{-1}\ s^{-1}$, which is only one order of magnitude higher than the experimental values of 0.3 to 0.5 $cm^2\ V^{-1}\ s^{-1}$.[248] Here, crystallinity is found not to be very important since mobilities in crystalline and the most disordered C_{60} are evaluated to differ only by a factor of 2; this result has been attributed to the efficient packing of C_{60} because of its spherical shape.[247]

MacKenzie et al.[249] have used MD simulations to investigate the molecular packing structure in solution-cast films of fullerene derivatives with different chain lengths; the addition of a side chain is seen to disrupt the packing of C_{60} molecules and introduces energetic disorder. The side chains push apart the C_{60} molecules, reducing the number of closely packed molecules and thus the number of molecules that can most electronically interact; as a result, the calculated electron mobilities are strongly decreased. The authors find an inverse dependence of mobility on electric field as well as a dependence on hydrocarbon chain length, i.e., the reduction in mobility is larger at high electric fields for a longer chain than for a shorter chain; in such a situation, charge carriers are increasingly forced to move exclusively along the direction of the electric field and more efficient pathways cannot contribute to carrier transport.

In their work, Tummala et al.[250] focused on the properties of various $PC_{61}BM$ aggregation structures using MD simulations. The authors derived molecular packing structures and charge transfer integrals, which then served as input into KMC simulations of the electron mobilities. They find that the intermolecular interactions in crystalline structures are influenced

by the inclusion of solvent molecules, which impacts the orientations of neighboring $PC_{61}BM$ molecules and the overall packing structure. As a result, the calculated electron mobilities are different; for the triclinic co-crystal of $PC_{61}BM$ with chlorobenzene, the largest electronmobility is about 0.2 $cm^2\ V^{-1}\ s^{-1}$, while for the monoclinic co-crystal with *o*-dichlorobenzene, the largest mobility is about twice smaller. The electron mobilities in amorphous $PC_{61}BM$s are evaluated to be ca. one order of magnitude lower than those in the crystalline structures, which is consistent with the effects of increasing disorder described by Nelson et al.[245] A reason for this reduction is that adjacent $PC_{61}BM$s that have strong intermolecular electronic couplings are not oriented along a specific path; also, the Coulombic repulsion among charge carriers, which limits charge carrier motion, is seen to have a much larger impact in amorphous systems, where there exist fewer efficient charge transport pathways. These results have been confirmed by Idé et al.[55] in their KMC simulations of the charge transport properties of $PC_{61}BM$ and $ThC_{61}BM$ (where the phenyl ring of the butyric acid methyl ester is replaced with a thienyl ring) in different crystal morphologies. Depending on the distribution of inter-fullerene distances, charge transport can vary from one- to two- to three-dimensional as a function of the crystal structure.

Moving towards the device scale, Steiner et al.[251] have used a multiscale modeling approach where coarse-grained MD simulations of fullerene derivatives (which enables the modeling of 100 000 molecules in a given system) are combined with quantum chemical estimates of the site energies, and KMC simulations to calculate the charge-carrier mobilities in $PC_{61}BM$, bis-$PC_{61}BM$ and tris-$PC_{61}BM$. The objective was to better understand the reasons for reduced mobility as the number of adducts increases. They find that the energetic disorder introduced as the number of phenyl-butyric acid methyl ester groups increases, is the main contributor to the reduction in carrier mobilities rather than packing disorder, which they attribute to the spherical symmetry of the C_{60} cage. However, it should be noted that Tummala et al.[250] have demonstrated that the electronic couplings between adjacent fullerenes can span from 0 meV to several hundred meV as one fullerene is rotated around its neighbor; this result calls into question the assumption that the spherical symmetry of the fullerenes necessarily results in isotropic interactions among neighbors.

5. Outlook

With single-junction OSCs now reaching nearly 12% efficiency, a comprehensive theoretical understanding of the electronic processes that occur within the active layer of these devices is necessary if we are to continue making significant progress towards higher power conversion efficiencies. As this review amply illustrates, the simple consideration of one acceptor molecule and one donor molecule is not sufficient to provide adequate insight into the complex interactions that occur at the interfaces between the donor and acceptor materials. Recent theoretical works demonstrate that the specific interactions among the molecular (or polymer) species and the overall effect of the molecular environment can result in qualitative changes in the description of a given system with respect to its analog in vacuum. Importantly, the energetics associated with specific sites do evolve substantially as a function of time, which underlines the impact of the system dynamics. Thus, a feedback approach is necessary wherein experimental investigations, that are able to sample time scales not easily accessible via theoretical methods and that can provide accurate measures of the properties of real systems, and theoretical investigations, that can provide molecular level insight into the system order and processes, complement and build upon each other.

From the computational and theoretical understanding that has been reached of OSC devices, a clear message arises. To accurately model these complex systems, a truly multiscale approach is needed, which combines the ability to accurately describe the interactions among molecular species, the effects of the molecular environment well beyond just a few neighboring molecules, the evolution of the system in time, and the ability to explicitly consider enough sites that relevant statistics may be obtained. While a single unifying model that is able to meet each of these requirements for all of the processes taking place in OSCs has yet to be realized, efforts are currently underway to investigate at least the individual processes on the basis of such methodologies.

Acknowledgements

This work has been supported by competitive research funding at King Abdullah University of Science and Technology (KAUST) and by ONR Global (Award N62909-15-1-2003). We thank KAUST IT Research Computing and the KAUST Supercomputing Laboratory for providing continuous assistance as well as ample computational and storage resources. S.R. thanks Dr. Tonghui Wang for providing structures for the Table of Contents graphic.

Received: June 23, 2016
Revised: July 25, 2016
Published online:

[1] J. Zhao, Y. Li, G. Yang, K. Jiang, H. Lin, H. Ade, W. Ma, H. Yan, *Nat. Energy* **2016**, *1*, 15027.
[2] Heliatek Heliatek Sets New Organic Photovoltaic World Record Efficiency of 13.2%. http://www.heliatek.com/en/press/press-releases/details/heliatek-sets-new-organic-photovoltaic-world-record-efficiency-of-13-2 (accessed March 7).
[3] NREL NREL Best Research-Cell Efficiencies. http://www.nrel.gov/ncpv/images/efficiency_chart.jpg (accessed April 13).
[4] H. Bin, Z.-G. Zhang, L. Gao, S. Chen, L. Zhong, L. Xue, C. Yang, Y. Li, *J. Am. Chem. Soc.* **2016**, *138*, 4657.
[5] V. Gupta, A. K. K. Kyaw, D. H. Wang, S. Chand, G. C. Bazan, A. J. Heeger, *Sci. Rep.* **2013**, *3*, 1965.
[6] Author, in *Organic Semiconductors: Manipulation and Control of the Microstructure of Active Layers*, Vol. *2* (Eds: S. R. Marder, J.-L. Brédas), World Scientific Publishing Co Pte Ltd, Singapore **2016**.
[7] J. L. Bredas, J. E. Norton, J. Cornil, V. Coropceanu, *Acc. Chem. Res.* **2009**, *42*, 1691.
[8] B. Kippelen, J. L. Bredas, *Energy Envir. Sci.* **2009**, *2*, 251.
[9] V. Coropceanu, J. Cornil, D. A. d. Silva, Y. Olivier, R. Silbey, J. L. Bredas, *Chem. Rev.* **2007**, *107*, 926.
[10] S. Verlaak, P. Heremans, *Phys. Rev. B* **2007**, *75*, 115127.

[11] S. Difley, L.-P. Wang, S. Yeganeh, S. R. Yost, T. V. Voorhis, *Acc. Chem. Res.* **2010**, *43*, 995.
[12] G. Horowitz, *Adv. Mater.* **1998**, *10*, 365.
[13] S. E. Fritz, S. M. Martin, C. D. Frisbie, M. D. Ward, M. F. Toney, *J. Am. Chem. Soc.* **2004**, *126*, 4084.
[14] E. F. Valeev, V. Coropceanu, D. A. da Silva Filho, S. Salman, J.-L. Brédas, *J. Am. Chem. Soc.* **2006**, *128*, 9882.
[15] V. Podzorov, E. Menard, A. Borissov, V. Kiryukhin, J. A. Rogers, M. E. Gershenson, *Phys. Rev. Lett.* **2004**, *93*, 086602.
[16] N. S. Sariciftci, L. Smilowitz, A. J. Heeger, F. Wudl, *Science* **1992**, *258*, 1474.
[17] A. J. Heeger, *Adv. Mater.* **2014**, *26*, 10.
[18] J.-L. Bredas, *Mater. Horiz.* **2014**, *1*, 17.
[19] T. M. Clarke, J. R. Durrant, *Chem. Rev.* **2010**, *110*, 6736.
[20] Author, in *Organic Photovoltaics: Physical Concepts Behind Device Operation*, Vol. *2* (Eds: S. R. Marder, J.-L. Brédas), World Scientific Publishing Co Pte Ltd, Singapore **2016**.
[21] T. M. Burke, S. Sweetnam, K. Vandewal, M. D. McGehee, *Adv. Energy Mater.* **2015**, *5*, 1500123.
[22] K. Vandewal, K. Tvingstedt, A. Gadisa, O. Inganas, J. V. Manca, *Nat. Mater.* **2009**, *8*, 904.
[23] O. V. Mikhnenko, P. W. M. Blom, T.-Q. Nguyen, *Energy Envir. Sci.* **2015**, *8*, 1867.
[24] S. Günes, H. Neugebauer, N. S. Sariciftci, *Chem. Rev.* **2007**, *107*, 1324.
[25] G. Dennler, M. C. Scharber, C. J. Brabec, *Adv. Mater.* **2009**, *21*, 1323.
[26] P. W. M. Blom, V. D. Mihailetchi, L. J. A. Koster, D. E. Markov, *Adv. Mater.* **2007**, *19*, 1551.
[27] F. Laquai, D. Andrienko, R. Mauer, P. W. M. Blom, *Macromol. Rapid Commun.* **2015**, *36*, 1001.
[28] G. Yu, J. Gao, J. C. Hummelen, F. Wudl, A. J. Heeger, *Science* **1995**, *270*, 1789.
[29] J. J. M. Halls, K. Pichler, R. H. Friend, S. C. Moratti, A. B. Holmes, *Appl. Phys. Lett.* **1996**, *68*, 3120.
[30] J. J. M. Halls, C. A. Walsh, N. C. Greenham, E. A. Marseglia, R. H. Friend, S. C. Moratti, A. B. Holmes, *Nature* **1995**, *376*, 498.
[31] M. Knupfer, *Appl. Phys. A* **2003**, *77*, 623.
[32] Z. B. Henson, K. Mullen, G. C. Bazan, *Nat. Chem.* **2012**, *4*, 699.
[33] M. C. Scharber, D. Mühlbacher, M. Koppe, P. Denk, C. Waldauf, A. J. Heeger, C. J. Brabec, *Adv. Mater.* **2006**, *18*, 789.
[34] Y. Li, *Acc. Chem. Res.* **2012**, *45*, 723.
[35] R. D. McCullough, R. D. Lowe, M. Jayaraman, D. L. Anderson, *J. Org. Chem.* **1993**, *58*, 904.
[36] T.-A. Chen, X. Wu, R. D. Rieke, *J. Am. Chem. Soc.* **1995**, *117*, 233.
[37] E. E. Havinga, W. ten Hoeve, H. Wynberg, *Synth. Met.* **1993**, *55*, 299.
[38] E. E. Havinga, W. ten Hoeve, H. Wynberg, *Polym. Bull. (Berlin)* **1992**, *29*, 119.
[39] S. Roquet, A. Cravino, P. Leriche, O. Alévêque, P. Frère, J. Roncali, *J. Am. Chem. Soc.* **2006**, *128*, 3459.
[40] A. Cravino, P. Leriche, O. Alévêque, S. Roquet, J. Roncali, *Adv. Mater.* **2006**, *18*, 3033.
[41] J. L. Brédas, G. B. Street, B. Thémans, J. M. André, *J. Chem. Phys.* **1985**, *83*, 1323.
[42] C. Kanimozhi, M. Naik, N. Yaacobi-Gross, E. K. Burnett, A. L. Briseno, T. D. Anthopoulos, S. Patil, *J. Phys. Chem. C* **2014**, *118*, 11536.
[43] D. A. Kislitsyn, B. N. Taber, C. F. Gervasi, L. Zhang, S. C. B. Mannsfeld, J. S. Prell, A. L. Briseno, G. V. Nazin, *Phys. Chem. Chem. Phys.* **2016**, *18*, 4842.
[44] J.-S. Wu, S.-W. Cheng, Y.-J. Cheng, C.-S. Hsu, *Chem. Soc. Rev.* **2015**, *44*, 1113.
[45] J. Mei, Z. Bao, *Chem. Mater.* **2014**, *26*, 604.
[46] A. El Labban, J. Warnan, C. Cabanetos, O. Ratel, C. Tassone, M. F. Toney, P. M. Beaujuge, *ACS Appl. Mater. Interfaces* **2014**, *6*, 19477.
[47] H. Hu, K. Jiang, G. Yang, J. Liu, Z. Li, H. Lin, Y. Liu, J. Zhao, J. Zhang, F. Huang, Y. Qu, W. Ma, H. Yan, *J. Am. Chem. Soc.* **2015**, *137*, 14149.
[48] N. Martin, *Chem. Commun.* **2013**, *49*, 1039.
[49] H. W. Kroto, J. R. Heath, S. C. O'Brien, R. F. Curl, R. E. Smalley, *Nature* **1985**, *318*, 162.
[50] N. E. Jackson, B. M. Savoie, L. X. Chen, M. A. Ratner, *J. Phys. Chem. Lett.* **2015**, *6*, 1018.
[51] T. Liu, A. Troisi, *Adv. Mater.* **2013**, *25*, 1038.
[52] P. J. Skabara, J.-B. Arlin, Y. H. Geerts, *Adv. Mater.* **2013**, *25*, 1948.
[53] N. R. Monahan, K. W. Williams, B. Kumar, C. Nuckolls, X. Y. Zhu, *Phys. Rev. Lett.* **2015**, *114*, 247003.
[54] B. A. Gregg, *J. Phys. Chem. Lett.* **2011**, *2*, 3013.
[55] J. Ide, D. Fazzi, M. Casalegno, S. V. Meille, G. Raos, *J. Mater. Chem. C* **2014**, *2*, 7313.
[56] J. C. Hummelen, B. W. Knight, F. LePeq, F. Wudl, J. Yao, C. L. Wilkins, *J. Org. Chem.* **1995**, *60*, 532.
[57] G. D'Avino, Y. Olivier, L. Muccioli, D. Beljonne, *J. Mater. Chem. C* **2016**, *4*, 3747.
[58] C. F. N. Marchiori, M. Koehler, *J. Phys. D: Appl. Phys.* **2014**, *47*, 215104.
[59] Y. Huang, E. J. Kramer, A. J. Heeger, G. C. Bazan, *Chem. Rev.* **2014**, *114*, 7006.
[60] R. Gonzalez, J. C. Hummelen, F. Wudl, *J. Org. Chem.* **1995**, *60*, 2618.
[61] L. Zheng, Q. Zhou, X. Deng, M. Yuan, G. Yu, Y. Cao, *J. Phys. Chem. B* **2004**, *108*, 11921.
[62] M. Seri, E. Rossi, T. Carofiglio, S. Antonello, G. Ruani, M. Maggini, M. Muccini, *J. Mater. Chem.* **2011**, *21*, 18308.
[63] F. B. Kooistra, J. Knol, F. Kastenberg, L. M. Popescu, W. J. H. Verhees, J. M. Kroon, J. C. Hummelen, *Org. Lett.* **2007**, *9*, 551.
[64] P. A. Troshin, H. Hoppe, J. Renz, M. Egginger, J. Y. Mayorova, A. E. Goryachev, A. S. Peregudov, R. N. Lyubovskaya, G. Gobsch, N. S. Sariciftci, V. F. Razumov, *Adv. Funct. Mater.* **2009**, *19*, 779.
[65] M. M. Wienk, J. M. Kroon, W. J. H. Verhees, J. Knol, J. C. Hummelen, P. A. van Hal, R. A. J. Janssen, *Angew. Chem., Int. Ed.* **2003**, *42*, 3371.
[66] E. Espíldora, J. L. Delgado, N. Martín, *Isr. J. Chem.* **2014**, *54*, 429.
[67] D. M. Guldi, B. M. Illescas, C. M. Atienza, M. Wielopolski, N. Martin, *Chem. Soc. Rev.* **2009**, *38*, 1587.
[68] Y. He, H.-Y. Chen, J. Hou, Y. Li, *J. Am. Chem. Soc.* **2010**, *132*, 1377.
[69] M. Lenes, G.-J. A. H. Wetzelaer, F. B. Kooistra, S. C. Veenstra, J. C. Hummelen, P. W. M. Blom, *Adv. Mater.* **2008**, *20*, 2116.
[70] M. Lenes, S. W. Shelton, A. B. Sieval, D. F. Kronholm, J. C. Hummelen, P. W. M. Blom, *Adv. Funct. Mater.* **2009**, *19*, 3002.
[71] B. Zhang, J. M. White, D. J. Jones, W. W. H. Wong, *Org. Biomol. Chem.* **2015**, *13*, 10505.
[72] Z. Xiao, X. Geng, D. He, X. Jia, L. Ding, *Energy Envir. Sci.* **2016**, *9*, 2114.
[73] C. Thilgen, F. Diederich, *Chem. Rev.* **2006**, *106*, 5049.
[74] F. Diederich, R. Kessinger, *Acc. Chem. Res.* **1999**, *32*, 537.
[75] M. R. Cerón, L. Echegoyen, *J. Phys. Org. Chem.* **2016**, 10.1002/poc.3563.
[76] B. Zhang, J. Subbiah, Y.-Y. Lai, J. M. White, D. J. Jones, W. W. H. Wong, *Chem. Commun.* **2015**, *51*, 9837.
[77] A. Sánchez-Díaz, M. Izquierdo, S. Filippone, N. Martin, E. Palomares, *Adv. Funct. Mater.* **2010**, *20*, 2695.
[78] N. C. Cates, R. Gysel, Z. Beiley, C. E. Miller, M. F. Toney, M. Heeney, I. McCulloch, M. D. McGehee, *Nano Lett.* **2009**, *9*, 4153.

[79] H. Azimi, A. Senes, M. C. Scharber, K. Hingerl, C. J. Brabec, *Adv. Energy Mater.* **2011**, *1*, 1162.
[80] M. A. Faist, S. Shoaee, S. Tuladhar, G. F. A. Dibb, S. Foster, W. Gong, T. Kirchartz, D. D. C. Bradley, J. R. Durrant, J. Nelson, *Adv. Energy Mater.* **2013**, *3*, 744.
[81] N. R. Tummala, Z. Zheng, S. G. Aziz, V. Coropceanu, J.-L. Brédas, *J. Phys. Chem. Lett.* **2015**, *6*, 3657.
[82] C. B. Nielsen, S. Holliday, H.-Y. Chen, S. J. Cryer, I. McCulloch, *Acc. Chem. Res.* **2015**, *48*, 2803.
[83] C. Zhan, J. Yao, *Chem. Mater.* **2016**, *28*, 1948.
[84] C. Li, H. Wonneberger, *Adv. Mater.* **2012**, *24*, 613.
[85] X. Zhan, A. Facchetti, S. Barlow, T. J. Marks, M. A. Ratner, M. R. Wasielewski, S. R. Marder, *Adv. Mater.* **2011**, *23*, 268.
[86] H. Benten, D. Mori, H. Ohkita, S. Ito, *J. Mater. Chem. A* **2016**, *4*, 5340.
[87] Z. Chen, Y. Zheng, H. Yan, A. Facchetti, *J. Am. Chem. Soc.* **2009**, *131*, 8.
[88] Y. Zhong, M. T. Trinh, R. Chen, G. E. Purdum, P. P. Khlyabich, M. Sezen, S. Oh, H. Zhu, B. Fowler, B. Zhang, W. Wang, C.-Y. Nam, M. Y. Sfeir, C. T. Black, M. L. Steigerwald, Y.-L. Loo, F. Ng, X. Y. Zhu, C. Nuckolls, *Nat. Commun.* **2015**, *6*, 8242.
[89] X. Zhang, Z. Lu, L. Ye, C. Zhan, J. Hou, S. Zhang, B. Jiang, Y. Zhao, J. Huang, S. Zhang, Y. Liu, Q. Shi, Y. Liu, J. Yao, *Adv. Mater.* **2013**, *25*, 5791.
[90] Y. Lin, X. Zhan, *Mater. Horiz.* **2014**, *1*, 470.
[91] A. Facchetti, *Mater. Today* **2013**, *16*, 123.
[92] P. Sonar, J. P. Fong Lim, K. L. Chan, *Ener. Envir. Sci.* **2011**, *4*, 1558.
[93] A. a. F. Eftaiha, J.-P. Sun, I. G. Hill, G. C. Welch, *J. Mater. Chem. A* **2014**, *2*, 1201.
[94] I. Salzmann, S. Duhm, G. Heimel, J. P. Rabe, N. Koch, M. Oehzelt, Y. Sakamoto, T. Suzuki, *Langmuir* **2008**, *24*, 7294.
[95] Y. Zang, C.-Z. Li, C.-C. Chueh, S. T. Williams, W. Jiang, Z.-H. Wang, J.-S. Yu, A. K. Y. Jen, *Adv. Mater.* **2014**, *26*, 5708.
[96] B. A. Jones, A. Facchetti, M. R. Wasielewski, T. J. Marks, *J. Am. Chem. Soc.* **2007**, *129*, 15259.
[97] P. Cheng, L. Ye, X. Zhao, J. Hou, Y. Li, X. Zhan, *Ener. Envir. Sci.* **2014**, *7*, 1351.
[98] Y. Lin, H. Wang, Y. Li, D. Zhu, X. Zhan, *J. Mater. Chem. A* **2013**, *1*, 14627.
[99] J. T. Bloking, X. Han, A. T. Higgs, J. P. Kastrop, L. Pandey, J. E. Norton, C. Risko, C. E. Chen, J.-L. Brédas, M. D. McGehee, A. Sellinger, *Chem. Mater.* **2011**, *23*, 5484.
[100] C. H. Woo, T. W. Holcombe, D. A. Unruh, A. Sellinger, J. M. J. Fréchet, *Chem. Mater.* **2010**, *22*, 1673.
[101] P. E. Schwenn, K. Gui, A. M. Nardes, K. B. Krueger, K. H. Lee, K. Mutkins, H. Rubinstein-Dunlop, P. E. Shaw, N. Kopidakis, P. L. Burn, P. Meredith, *Adv. Energy Mater.* **2011**, *1*, 73.
[102] X. Liu, S. Huettner, Z. Rong, M. Sommer, R. H. Friend, *Adv. Mater.* **2012**, *24*, 669.
[103] D. Mori, H. Benten, H. Ohkita, S. Ito, K. Miyake, *ACS Appl. Mater. Interfaces* **2012**, *4*, 3325.
[104] C. R. McNeill, A. Abrusci, J. Zaumseil, R. Wilson, M. J. McKiernan, J. H. Burroughes, J. J. M. Halls, N. C. Greenham, R. H. Friend, *Appl. Phys. Lett.* **2007**, *90*, 193506.
[105] S. Nam, M. Shin, S. Park, S. Lee, H. Kim, Y. Kim, *Phys. Chem. Chem. Phys.* **2012**, *14*, 15046.
[106] Y. Kim, S. Cook, S. A. Choulis, J. Nelson, J. R. Durrant, D. D. C. Bradley, *Chem. Mater.* **2004**, *16*, 4812.
[107] S. Holliday, R. S. Ashraf, C. B. Nielsen, M. Kirkus, J. A. Röhr, C.-H. Tan, E. Collado-Fregoso, A.-C. Knall, J. R. Durrant, J. Nelson, I. McCulloch, *J. Am. Chem. Soc.* **2015**, *137*, 898.
[108] S. Holliday, R. S. Ashraf, A. Wadsworth, D. Baran, S. A. Yousaf, C. B. Nielsen, C.-H. Tan, S. D. Dimitrov, Z. Shang, N. Gasparini, M. Alamoudi, F. Laquai, C. J. Brabec, A. Salleo, J. R. Durrant, I. McCulloch, *Nat. Commun.* **2016**, *7*, 11585.
[109] Y. Shu, Y.-F. Lim, Z. Li, B. Purushothaman, R. Hallani, J. E. Kim, S. R. Parkin, G. G. Malliaras, J. E. Anthony, *Chem. Sci.* **2011**, *2*, 363.
[110] Z. Li, Y.-F. Lim, J. B. Kim, S. R. Parkin, Y.-L. Loo, G. G. Malliaras, J. E. Anthony, *Chem. Commun.* **2011**, *47*, 7617.
[111] T. Zhou, T. Jia, B. Kang, F. Li, M. Fahlman, Y. Wang, *Adv. Energy Mater.* **2011**, *1*, 431.
[112] K. N. Winzenberg, P. Kemppinen, F. H. Scholes, G. E. Collis, Y. Shu, T. Birendra Singh, A. Bilic, C. M. Forsyth, S. E. Watkins, *Chem. Commun.* **2013**, *49*, 6307.
[113] F. G. Brunetti, X. Gong, M. Tong, A. J. Heeger, F. Wudl, *Angew. Chem., Int. Ed.* **2010**, *49*, 532.
[114] K. Cnops, B. P. Rand, D. Cheyns, B. Verreet, M. A. Empl, P. Heremans, *Nat. Commun.* **2014**, *5*, 3406.
[115] J. Min, Z.-G. Zhang, S. Zhang, Y. Li, *Chem. Mater.* **2012**, *24*, 3247.
[116] L. Gao, Z.-G. Zhang, L. Xue, J. Min, J. Zhang, Z. Wei, Y. Li, *Adv. Mater.* **2016**, *28*, 1884.
[117] Y. Lin, P. Cheng, Y. Li, X. Zhan, *Chem. Commun.* **2012**, *48*, 4773.
[118] Y. Yi, V. Coropceanu, J.-L. Brédas, *J. Am. Chem. Soc.* **2009**, *131*, 15777.
[119] J. Idé, S. Mothy, A. Savoyant, A. Fritsch, P. Aurel, R. Méreau, L. Ducasse, J. Cornil, D. Beljonne, F. Castet, *Int. J. Quantum Chem.* **2013**, *113*, 580.
[120] W. Chen, D.-C. Qi, H. Huang, X. Gao, A. T. S. Wee, *Adv. Funct. Mater.* **2011**, *21*, 410.
[121] G. D'Avino, L. Muccioli, Y. Olivier, D. Beljonne, *J. Phys. Chem. Lett.* **2016**, *7*, 536.
[122] P. Gemünden, C. Poelking, K. Kremer, K. Daoulas, D. Andrienko, *Macromol. Rapid Commun.* **2015**, *36*, 1047.
[123] C. Poelking, M. Tietze, C. Elschner, S. Olthof, D. Hertel, B. Baumeier, F. Würthner, K. Meerholz, K. Leo, D. Andrienko, *Nat. Mater.* **2015**, *14*, 434.
[124] B. A. Collins, Z. Li, J. R. Tumbleston, E. Gann, C. R. McNeill, H. Ade, *Adv. Energy Mater.* **2013**, *3*, 65.
[125] S. Mukherjee, C. M. Proctor, G. C. Bazan, T.-Q. Nguyen, H. Ade, *Adv. Energy Mater.* **2015**, *5*, 1500877.
[126] B. P. Lyons, N. Clarke, C. Groves, *Ener. Envir. Sci.* **2012**, *5*, 7657.
[127] J. A. Bartelt, Z. M. Beiley, E. T. Hoke, W. R. Mateker, J. D. Douglas, B. A. Collins, J. R. Tumbleston, K. R. Graham, A. Amassian, H. Ade, J. M. J. Fréchet, M. F. Toney, M. D. McGehee, *Adv. Energy Mater.* **2013**, *3*, 364.
[128] B. M. Savoie, K. L. Kohlstedt, N. E. Jackson, L. X. Chen, M. Olvera de la Cruz, G. C. Schatz, T. J. Marks, M. A. Ratner, *Proc. Natl. Acad. Sci.* **2014**, *111*, 10055.
[129] N. E. Jackson, L. X. Chen, M. A. Ratner, *Proc. Natl. Acad. Sci.* **2016**, *113*, 8595.
[130] B. H. Wunsch, M. Rumi, N. R. Tummala, C. Risko, D.-Y. Kang, K. X. Steirer, J. Gantz, M. Said, N. R. Armstrong, J.-L. Bredas, D. Bucknall, S. R. Marder, *J. Mater. Chem. C* **2013**, *1*, 5250.
[131] W. Ma, J. R. Tumbleston, L. Ye, C. Wang, J. Hou, H. Ade, *Adv. Mater.* **2014**, *26*, 4234.
[132] F. Dou, E. Buchaca-Domingo, M. Sakowicz, E. Rezasoltani, T. McCarthy-Ward, M. Heeney, X. Zhang, N. Stingelin, C. Silva, *J. Mater. Chem. C* **2015**, *3*, 3722.
[133] R. Noriega, J. Rivnay, K. Vandewal, F. P. V. Koch, N. Stingelin, P. Smith, M. F. Toney, A. Salleo, *Nat. Mater.* **2013**, *12*, 1038.
[134] P. Westacott, J. R. Tumbleston, S. Shoaee, S. Fearn, J. H. Bannock, J. B. Gilchrist, S. Heutz, J. deMello, M. Heeney, H. Ade, J. Durrant, D. S. McPhail, N. Stingelin, *Energy Envir. Sci.* **2013**, *6*, 2756.
[135] E. Buchaca-Domingo, K. Vandewal, Z. Fei, S. E. Watkins, F. H. Scholes, J. H. Bannock, J. C. de Mello, L. J. Richter, D. M. DeLongchamp, A. Amassian, M. Heeney, A. Salleo, N. Stingelin, *J. Am. Chem. Soc.* **2015**, *137*, 5256.
[136] H. Yan, S. Swaraj, C. Wang, I. Hwang, N. C. Greenham, C. Groves, H. Ade, C. R. McNeill, *Adv. Funct. Mater.* **2010**, *20*, 4329.

[137] B. A. Collins, J. R. Tumbleston, H. Ade, *J. Phys. Chem. Lett.* **2011**, *2*, 3135.
[138] W. Chen, M. P. Nikiforov, S. B. Darling, *Energy Envir. Sci.* **2012**, *5*, 8045.
[139] S. Sweetnam, K. R. Graham, G. O. Ngongang Ndjawa, T. Heumüller, J. A. Bartelt, T. M. Burke, W. Li, W. You, A. Amassian, M. D. McGehee, *J. Am. Chem. Soc.* **2014**, *136*, 14078.
[140] S. Sweetnam, K. Vandewal, E. Cho, C. Risko, V. Coropceanu, A. Salleo, J.-L. Brédas, M. D. McGehee, *Chem. Mater.* **2016**, *28*, 1446.
[141] C. Grand, S. Baek, T.-H. Lai, N. Deb, W. Zajaczkowski, R. Stalder, K. Müllen, W. Pisula, D. G. Bucknall, F. So, J. R. Reynolds, *Macromolecules* **2016**, *49*, 4008.
[142] T.-H. Lai, I. Constantinou, C. M. Grand, E. D. Klump, S. Baek, H.-Y. Hsu, S.-W. Tsang, K. S. Schanze, J. R. Reynolds, F. So, *Chem. Mater.* **2016**, *28*, 2433.
[143] K. R. Graham, C. Cabanetos, J. P. Jahnke, M. N. Idso, A. El Labban, G. O. Ngongang Ndjawa, T. Heumueller, K. Vandewal, A. Salleo, B. F. Chmelka, A. Amassian, P. M. Beaujuge, M. D. McGehee, *J. Am. Chem. Soc.* **2014**, *136*, 9608.
[144] C. Dyer-Smith, I. A. Howard, C. Cabanetos, A. El Labban, P. M. Beaujuge, F. Laquai, *Adv. Energy Mater.* **2015**, *5*, 1401778.
[145] C. B. Nielsen, R. S. Ashraf, N. D. Treat, B. C. Schroeder, J. E. Donaghey, A. J. P. White, N. Stingelin, I. McCulloch, *Adv. Mater.* **2015**, *27*, 948.
[146] M. K. Ravva, T. Wang, J. L. Brédas, *Unpublished Work* **2016**.
[147] T. Wang, M. K. Ravva, J.-L. Brédas, *Adv. Funct. Mater.* **2016**, 10.1002/adfm.201601134.
[148] B. Yang, Y. Yi, C.-R. Zhang, S. G. Aziz, V. Coropceanu, J.-L. Brédas, *J. Phys. Chem. C* **2014**, *118*, 27648.
[149] S. Sharifzadeh, A. Biller, L. Kronik, J. B. Neaton, *Phys. Rev. B* **2012**, *85*, 125307.
[150] E. A. Silinsh, *Organic Molecular Crystals: Their Electronic States*, Springer, New York **1980**.
[151] E. A. Silinsh, V. Čápek, Organic Molecular Crystals: Interaction, Localization, and Transport Phenomena, **1994**.
[152] M. Pope, C. E. Swenberg, Electronic Processes in Organic Crystals and Polymers, **1999**.
[153] N. Sato, K. Seki, H. Inokuchi, *J. Chem. Soc., Faraday Trans. 2* **1981**, *77*, 1621.
[154] N. Sato, H. Inokuchi, E. A. Silinsh, *Chem. Phys.* **1987**, *115*, 269.
[155] L. Lyons, *Aust. J. Chem.* **1957**, *10*, 365.
[156] H. Yoshida, K. Yamada, J. y. Tsutsumi, N. Sato, *Phys. Rev. B* **2015**, *92*, 075145.
[157] G. D'Avino, L. Muccioli, F. Castet, C. Poelking, D. Andrienko, Z. G. Soos, J. Cornil, D. Beljonne, *J. Phys.: Condens. Matter* **2016**, accepted.
[158] M. Born, *Z. Phys.* **1920**, *1*, 45.
[159] R. Firouzi, M. Zahedi, *J. Mol. Struct. Theochem.* **2008**, *862*, 7.
[160] L. M. Ramaniah, S. V. Nair, K. C. Rustagi, *Opt. Commun.* **1993**, *96*, 289.
[161] Z. Shuai, J. L. Brédas, *Phys. Rev. B* **1992**, *46*, 16135.
[162] M. Batley, L. Johnston, L. Lyons, *Aust. J. Chem.* **1970**, *23*, 2397.
[163] P. J. Bounds, R. W. Munn, *Chem. Phys.* **1979**, *44*, 103.
[164] P. J. Bounds, R. W. Munn, *Chem. Phys.* **1981**, *59*, 47.
[165] S. Verlaak, D. Beljonne, D. Cheyns, C. Rolin, M. Linares, F. Castet, J. Cornil, P. Heremans, *Adv. Funct. Mater.* **2009**, *19*, 3809.
[166] M. Linares, D. Beljonne, J. r. m. Cornil, K. Lancaster, J.-L. Brédas, S. Verlaak, A. Mityashin, P. Heremans, A. Fuchs, C. Lennartz, J. Idé, R. l. Méreau, P. Aurel, L. Ducasse, F. d. r. Castet, *J. Phys. Chem. C* **2010**, *114*, 3215.
[167] G. D'Avino, L. Muccioli, C. Zannoni, D. Beljonne, Z. G. Soos, *J. Chem. Theory Comput.* **2014**, *10*, 4959.
[168] S. M. Ryno, S. R. Lee, J. Sears, C. Risko, J. L. Bredas, *J. Phys. Chem. C* **2013**, *117*, 13853.
[169] A. J. Stone, *Mol. Phys.* **1985**, *56*, 1065.
[170] A. J. Stone, *The Theory of Intermolecular Forces*, Clarendon Press, Oxford **1996**.
[171] Z. G. Soos, E. V. Tsiper, R. A. Pascal Jr., *Chem. Phys. Lett.* **2001**, *342*, 652.
[172] J. M. Sin, E. V. Tsiper, Z. G. Soos, *Europhys. Lett.* **2002**, *60*, 743.
[173] A. Morita, S. Kato, *J. Am. Chem. Soc.* **1997**, *119*, 4021.
[174] A. Morita, S. Kato, *J. Chem. Phys.* **1998**, *108*, 6809.
[175] S. Iuchi, A. Morita, S. Kato, *J. Phys. Chem. B* **2002**, *106*, 3466.
[176] J. y. Tsutsumi, H. Yoshida, R. Murdey, S. Kato, N. Sato, *J. Phys. Chem. A* **2009**, *113*, 9207.
[177] J. E. Norton, J.-L. Brédas, *J. Am. Chem. Soc.* **2008**, *130*, 12377.
[178] S. Refaely-Abramson, S. Sharifzadeh, M. Jain, R. Baer, J. B. Neaton, L. Kronik, *Phys. Rev. B* **2013**, *88*, 081204.
[179] P. Friederich, F. Symalla, V. Meded, T. Neumann, W. Wenzel, *J. Chem. Theory Comput.* **2014**, *10*, 3720.
[180] P. Petelenz, M. Snamina, G. Mazur, *J. Phys. Chem. C* **2015**, *119*, 14338.
[181] P. Friederich, V. Meded, F. Symalla, M. Elstner, W. Wenzel, *J. Chem. Theory Comput.* **2015**, *11*, 560.
[182] F. Castet, P. Aurel, A. Fritsch, L. Ducasse, D. Liotard, M. Linares, J. Cornil, D. Beljonne, *Phys. Rev. B* **2008**, *77*, 115210.
[183] L. E. Ratcliff, L. Grisanti, L. Genovese, T. Deutsch, T. Neumann, D. Danilov, W. Wenzel, D. Beljonne, J. Cornil, *J. Chem. Theory Comput.* **2015**, *11*, 2077.
[184] A. K. Rappe, C. J. Casewit, K. S. Colwell, W. A. Goddard, W. M. Skiff, *J. Am. Chem. Soc.* **1992**, *114*, 10024.
[185] N. Koch, A. Vollmer, S. Duhm, Y. Sakamoto, T. Suzuki, *Adv. Mater.* **2007**, *19*, 112.
[186] I. Salzmann, S. Duhm, G. Heimel, M. Oehzelt, R. Kniprath, R. L. Johnson, J. P. Rabe, N. Koch, *J. Am. Chem. Soc.* **2008**, *130*, 12870.
[187] G. Heimel, I. Salzmann, S. Duhm, N. Koch, *Chem. Mater.* **2010**, *23*, 359.
[188] S. M. Ryno, C. Risko, J.-L. Brédas, *J. Am. Chem. Soc.* **2014**, *136*, 6421.
[189] S. M. Ryno, C. Risko, J. L. Bredas, *ACS Appl. Mater. Interfaces* **2016**, *8*, 14053.
[190] W. Salaneck, *Phys. Rev. Lett.* **1978**, *40*, 60.
[191] E. V. Tsiper, Z. G. Soos, *Phys. Rev. B* **2003**, *68*, 085301.
[192] N. Gorczak, M. Swart, F. C. Grozema, *J. Mater. Chem. C* **2014**, *2*, 3467.
[193] D. Beljonne, J. Cornil, L. Muccioli, C. Zannoni, J. L. Bredas, F. Castet, *Chem. Mater.* **2011**, *23*, 591.
[194] S. Mothy, M. Guillaume, J. Idé, F. Castet, L. Ducasse, J. Cornil, D. Beljonne, *J. Phys. Chem. Lett.* **2012**, *3*, 2374.
[195] F. Castet, G. D'Avino, L. Muccioli, J. Cornil, D. Beljonne, *Phys. Chem. Chem. Phys.* **2014**, *16*, 20279.
[196] S. M. Ryno, Y. T. Fu, C. Risko, J. L. Bredas, *ACS Appl. Mater. Interfaces* **2016**, *8*, 15524.
[197] C. Poelking, D. Andrienko, *J. Am. Chem. Soc.* **2015**, *137*, 6320.
[198] G. D'Avino, S. Mothy, L. Muccioli, C. Zannoni, L. Wang, J. Cornil, D. Beljonne, F. Castet, *J. Phys. Chem. C* **2013**, *117*, 12981.
[199] M. Huix-Rotllant, H. Tamura, I. Burghardt, *J. Phys. Chem. Lett.* **2015**, *6*, 1702.
[200] H. Tamura, I. Burghardt, *J. Am. Chem. Soc.* **2013**, *135*, 16364.
[201] S. R. Cowan, N. Banerji, W. L. Leong, A. J. Heeger, *Adv. Funct. Mater.* **2012**, *22*, 1116.
[202] A. A. Bakulin, A. Rao, V. G. Pavelyev, P. H. M. van Loosdrecht, M. S. Pshenichnikov, D. Niedzialek, J. Cornil, D. Beljonne, R. H. Friend, *Science* **2012**, *335*, 1340.
[203] S. Gélinas, A. Rao, A. Kumar, S. L. Smith, A. W. Chin, J. Clark, T. S. van der Poll, G. C. Bazan, R. H. Friend, *Science* **2014**, *343*, 512.

[204] B. M. Savoie, A. Rao, A. A. Bakulin, S. Gelinas, B. Movaghar, R. H. Friend, T. J. Marks, M. A. Ratner, *J. Am. Chem. Soc.* **2014**, *136*, 2876.
[205] B. Bernardo, D. Cheyns, B. Verreet, R. D. Schaller, B. P. Rand, N. C. Giebink, *Nat. Commun.* **2014**, *5*, 3245.
[206] D. L. Cheung, A. Troisi, *J. Phys. Chem. C* **2010**, *114*, 20479.
[207] R. A. Street, P. P. Khlyabich, A. E. Rudenko, B. C. Thompson, *J. Phys. Chem. C* **2014**, *118*, 26569.
[208] H. Tamura, I. Burghardt, *J. Phys. Chem. C* **2013**, *117*, 15020.
[209] T. Stein, L. Kronik, R. Baer, *J. Am. Chem. Soc.* **2009**, *131*, 2818.
[210] R. A. Street, *Adv. Mater.* **2016**, *28*, 3814.
[211] P. B. Deotare, W. Chang, E. Hontz, D. N. Congreve, L. Shi, P. D. Reusswig, B. Modtland, M. E. Bahlke, C. K. Lee, A. P. Willard, V. Bulovic, T. Van Voorhis, M. A. Baldo, *Nat. Mater.* **2015**, *14*, 1130.
[212] S. D. Collins, C. M. Proctor, N. A. Ran, T.-Q. Nguyen, *Adv. Energy Mater.* **2016**, *6*, 1501721.
[213] V. Coropceanu, J. Cornil, D. A. da Silva Filho, Y. Olivier, R. Silbey, J.-L. Brédas, *Chem. Rev.* **2007**, *107*, 926.
[214] B. Baumeier, D. Andrienko, M. Rohlfing, *J. Chem. Theory Comput.* **2012**, *8*, 2790.
[215] D. Niedzialek, I. Duchemin, T. B. de Queiroz, S. Osella, A. Rao, R. Friend, X. Blase, S. Kümmel, D. Beljonne, *Adv. Funct. Mater.* **2015**, *25*, 1972.
[216] D. Zhang, S. N. Steinmann, W. Yang, *J. Chem. Phys.* **2013**, *139*, 154109.
[217] I. Duchemin, X. Blase, *Phys. Rev. B* **2013**, *87*, 245412.
[218] C. A. Ullrich, *Time-Dependent Density-Functional Theory: Concepts and Applications*, Oxford University Press, New York **2012**.
[219] A. J. Cohen, P. Mori-Sánchez, W. Yang, *Science* **2008**, *321*, 792.
[220] J.-D. Chai, M. Head-Gordon, *Phys. Chem. Chem. Phys.* **2008**, *10*, 6615.
[221] O. A. Vydrov, J. Heyd, A. V. Krukau, G. E. Scuseria, *J. Chem. Phys.* **2006**, *125*, 074106.
[222] C. Faber, P. Boulanger, I. Duchemin, C. Attaccalite, X. Blase, *J. Chem. Phys.* **2013**, *139*, 194308.
[223] C. Faber, I. Duchemin, T. Deutsch, X. Blase, *Phys. Rev. B* **2012**, *86*, 155315.
[224] H. Yin, Y. Ma, J. Mu, C. Liu, M. Rohlfing, *Phys. Rev. Lett.* **2014**, *112*, 228301.
[225] B. Baumeier, M. Rohlfing, D. Andrienko, *J. Chem. Theory Comput.* **2014**, *10*, 3104.
[226] X. Blase, C. Attaccalite, *Appl. Phys. Lett.* **2011**, *99*, 171909.
[227] K. Vandewal, S. Albrecht, E. T. Hoke, K. R. Graham, J. Widmer, J. D. Douglas, M. Schubert, W. R. Mateker, J. T. Bloking, G. F. Burkhard, A. Sellinger, J. M. J. Fréchet, A. Amassian, M. K. Riede, M. D. McGehee, D. Neher, A. Salleo, *Nat. Mater.* **2014**, *13*, 63.
[228] S. R. Yost, T. Van Voorhis, *J. Phys. Chem. C* **2013**, *117*, 5617.
[229] Y.-T. Fu, C. Risko, J.-L. Brédas, *Adv. Mater.* **2013**, *25*, 878.
[230] M. E. Gershenson, V. Podzorov, A. F. Morpurgo, *Rev. Mod. Phys.* **2006**, *78*, 973.
[231] E. A. Silinsh, V. Capek, *Organic Molecular Crystals: Interaction, Localization, and Transport Phenomena*, AIP, New York **1994**.
[232] Author, in *Charge Transport in Crystalline Organic Semiconductors*, Vol. 1 (Eds: J.-L. Brédas, S. R. Marder), World Scientific Publishing Co Pte Ltd, Singapore **2016**.
[233] P. K. Watkins, A. B. Walker, G. L. B. Verschoor, *Nano Lett.* **2005**, *5*, 1814.
[234] R. A. Marsh, C. Groves, N. C. Greenham, *J. Appl. Phys.* **2007**, *101*, 083509.
[235] C. Groves, R. A. Marsh, N. C. Greenham, *J. Chem. Phys.* **2008**, *129*, 114903.
[236] C. Groves, L. J. A. Koster, N. C. Greenham, *J. Appl. Phys.* **2009**, *105*, 094510.
[237] C. Deibel, T. Strobel, V. Dyakonov, *Phys. Rev. Lett.* **2009**, *103*, 036402.
[238] L. Y. Meng, Y. Shang, Q. K. Li, Y. F. Li, X. W. Zhan, Z. G. Shuai, R. G. E. Kimber, A. B. Walker, *J. Phys. Chem. B* **2010**, *114*, 36.
[239] D. A. Vithanage, A. Devižis, V. Abramavičius, Y. Infahsaeng, D. Abramavičius, R. C. I. MacKenzie, P. E. Keivanidis, A. Yartsev, D. Hertel, J. Nelson, V. Sundström, V. Gulbinas, *Nat. Commun.* **2013**, *4*, 2334.
[240] C. Groves, *Ener. Envir. Sci.* **2013**, *6*, 1546.
[241] S. Shoaee, S. Mehraeen, J. G. Labram, J.-L. Brédas, D. D. C. Bradley, V. Coropceanu, T. D. Anthopoulos, J. R. Durrant, *J. Phys. Chem. Lett.* **2014**, *5*, 3669.
[242] V. Abramavicius, D. Amarasinghe Vithanage, A. Devizis, Y. Infahsaeng, A. Bruno, S. Foster, P. E. Keivanidis, D. Abramavicius, J. Nelson, A. Yartsev, V. Sundstrom, V. Gulbinas, *Phys. Chem. Chem. Phys.* **2014**, *16*, 2686.
[243] M. C. Heiber, C. Baumbach, V. Dyakonov, C. Deibel, *Phys. Rev. Lett.* **2015**, *114*, 136602.
[244] M. L. Jones, D. M. Huang, B. Chakrabarti, C. Groves, *J. Phys. Chem. C* **2016**, *120*, 4240.
[245] J. Nelson, J. J. Kwiatkowski, J. Kirkpatrick, J. M. Frost, *Acc. Chem. Res.* **2009**, *42*, 1768.
[246] J. J. Kwiatkowski, J. Nelson, H. Li, J. L. Bredas, W. Wenzel, C. Lennartz, *Phys. Chem. Chem. Phys.* **2008**, *10*, 1852.
[247] J. J. Kwiatkowski, J. M. Frost, J. Nelson, *Nano Lett.* **2009**, *9*, 1085.
[248] S. Kobayashi, T. Takenobu, S. Mori, A. Fujiwara, Y. Iwasa, *Appl. Phys. Lett.* **2003**, *82*, 4581.
[249] R. C. I. MacKenzie, J. M. Frost, J. Nelson, *J. Chem. Phys.* **2010**, *132*, 064904.
[250] N. R. Tummala, S. Mehraeen, Y.-T. Fu, C. Risko, J.-L. Brédas, *Adv. Funct. Mater.* **2013**, *23*, 5800.
[251] F. Steiner, S. Foster, A. Losquin, J. Labram, T. D. Anthopoulos, J. M. Frost, J. Nelson, *Mater. Horiz.* **2015**, *2*, 113.
[252] F. Zhang, M. Johansson, M. R. Andersson, J. C. Hummelen, O. Inganäs, *Adv. Mater.* **2002**, *14*, 662.
[253] Q. Zhang, B. Kan, F. Liu, G. Long, X. Wan, X. Chen, Y. Zuo, W. Ni, H. Zhang, M. Li, Z. Hu, F. Huang, Y. Cao, Z. Liang, M. Zhang, T. P. Russell, Y. Chen, *Nat. Photonics* **2015**, *9*, 35.
[254] J. C. Hummelen, B. W. Knight, F. LePeq, F. Wudl, J. Yao, C. L. Wilkins, *J. Org. Chem.* **1995**, *60*, 532.
[255] Y.-J. Hwang, B. A. E. Courtright, A. S. Ferreira, S. H. Tolbert, S. A. Jenekhe, *Adv. Mater.* **2015**, *27*, 4578.
[256] M. Pope, J. Burgos, J. Giachino, *J. Chem. Phys.* **1965**, *43*, 3367.
[257] N. Ando, M. Mitsui, A. Nakajima, *J. Chem. Phys.* **2008**, *128*, 154318.
[258] N. Sato, Y. Saito, H. Shinohara, *Chem. Phys.* **1992**, *162*, 433.
[259] H. Yoshida, *J. Phys. Chem. C* **2014**, *118*, 24377.